

**LA-6123-PR**

Progress Report

**C.3**

Special Distribution  
Issued: November 1975

**CIC-14 REPORT COLLECTION  
REPRODUCTION  
COPY**

**Applied Nuclear Data  
Research and Development**

**April 1—June 30, 1975**

Compiled by

**D. W. Muir  
P. G. Young**

LOS ALAMOS NATIONAL LABORATORY

3 9338 00365 3952



**los alamos  
scientific laboratory**

**of the University of California**

**LOS ALAMOS, NEW MEXICO 87545**

An Affirmative Action/Equal Opportunity Employer

**UNITED STATES  
ENERGY RESEARCH AND DEVELOPMENT ADMINISTRATION  
CONTRACT W-7405-ENG. 36**

The four most recent reports in this series, unclassified, are LA-5727-PR, LA-5804-PR, LA-5944-PR, and LA-6018-PR.

In the interest of prompt distribution, this report was not edited by the Technical Information staff.

This work was performed under the auspices of the Defense Nuclear Agency, the Nuclear Regulatory Commission, the National Aeronautics and Space Administration, and the U.S. Energy Research and Development Administration's Divisions of Military Application, Reactor Research and Development, Physical Research, and Controlled Thermonuclear Research.

This report was prepared as an account of work sponsored by the United States Government. Neither the United States nor the United States Energy Research and Development Administration, nor any of their employees, nor any of their contractors, subcontractors, or their employees, makes any warranty, express or implied, or assumes any legal liability or responsibility for the accuracy, completeness, or usefulness of any information, apparatus, product, or process disclosed, or represents that its use would not infringe privately owned rights.

CONTENTS

I.	THEORY AND EVALUATION OF NUCLEAR CROSS SECTIONS.....	1
A.	Thermonuclear Reaction Parameters for the $T(d,n)^4\text{He}$ and $^3\text{He}(d,p)^4\text{He}$ Reactions.....	1
B.	GNASH Code Development.....	1
C.	Calculation of $(n,xn)$ Cross Sections.....	2
D.	Evaluation of $^6\text{Li}$ Neutron Cross Sections Above 1 MeV.....	2
E.	Evaluation of $^{15}\text{N}$ Neutron Cross Sections.....	2
F.	Cross-Section Uncertainty Evaluation for $^{27}\text{Al}$ .....	3
G.	Time-Dependent Photon Spectra from Fission of $^{235}\text{U}$ and $^{239}\text{Pu}$ ....	3
H.	Development of ENDF/B Formats for Activation and Decay Data.....	3
II.	NUCLEAR-CROSS SECTION PROCESSING.....	4
A.	Cross-Section Production.....	4
B.	MINX Code Development.....	4
C.	NJOY Code Development.....	5
D.	Advanced Processing Theory.....	7
III.	PHASE II TESTING OF ENDF/B-IV DATA.....	8
A.	Phase II Results for Benchmark Criticals.....	8
B.	Discrepancies in Phase II Results.....	9
C.	GODIVA and JEZEBEL 26-Group Transport Calculations.....	10
IV.	NUCLEAR DATA PROCESSING FOR HTGR SAFETY RESEARCH.....	10
V.	NUCLEAR DATA FOR CTR APPLICATIONS.....	11
A.	Evaluation of Cross-Section Uncertainties for TFTR Data Assessment.....	11
B.	Error Processing.....	11
VI.	DATA ADJUSTMENT METHODS.....	12
A.	Techniques for Simultaneous Adjustment of Large Nuclear Data Libraries.....	12
B.	Matrix Formulation of Data Adjustment Methods.....	12
VII.	FISSION-PRODUCT YIELD AND RADIOACTIVE DECAY STUDIES.....	14
A.	CINDER Code Development.....	14
B.	ENDF/B-IV Data.....	14
C.	Energy Release from Gaseous and Solid Fission Products Following $^{235}\text{U}$ and $^{239}\text{Pu}$ Fission Bursts.....	15
D.	Fission-Product Gamma and Photoneutron Spectra and Energy-Integrated Time-Dependent Distributions.....	15
VIII.	MEDIUM-ENERGY LIBRARY.....	23
	REFERENCES.....	24
	PUBLICATIONS AND TALKS.....	25

LOS ALAMOS NATL LAB LIBS.



3 9338 00365 3952

APPLIED NUCLEAR DATA RESEARCH AND DEVELOPMENT

QUARTERLY PROGRESS REPORT

April 1 — June 30, 1975

Compiled by

D. W. Muir and P. G. Young

ABSTRACT

This progress report describes the activities of the Los Alamos Nuclear Data Group for the period April 1 through June 30, 1975. The topical content of this report is summarized in the Contents.

I. THEORY AND EVALUATION OF NUCLEAR CROSS SECTIONS

A. Thermonuclear Reaction Parameters for the T(d,n)<sup>4</sup>He and <sup>3</sup>He(d,p)<sup>4</sup>He Reactions (G. M. Hale and D. E. Del [Carnegie Mellon University])

Reaction parameters, or Maxwellian-averaged products of the reaction cross section times the relative velocity  $\langle\sigma v\rangle$ , are used extensively in the design of weapons and some Controlled Thermonuclear Reactor (CTR) devices. Of most interest are the deuteron-induced thermonuclear reactions T(d,n)<sup>4</sup>He, <sup>3</sup>He(d,p)<sup>4</sup>He, and D(d,p)T. In designs where the deuterons are thermalized at relatively low temperatures, the reaction parameters are determined primarily by the cross sections at low energies, where the difficulty of the measurements render experimental values uncertain or nonexistent. One must generally rely on theoretical extrapolations to give values of the cross sections in this low energy region ( $E_d < 20$  keV).

A particularly appropriate method for representing the cross sections at all energies comes from the R-matrix theory of nuclear reactions,<sup>1</sup> since this theory takes proper account of resonances in addition to the usual barrier penetration effects. This is especially important in the case of the T(d,n) and <sup>3</sup>He(d,p) reactions, which are dominated by a large resonance at low energies.

We have used the cross sections calculated from such an analysis,<sup>2</sup> which considers the T(d,n) and <sup>3</sup>He(d,p) reactions simultaneously in a charge-inde-

pendent framework, to generate reaction parameters for D-T and D-<sup>3</sup>He reactions at temperatures between 0.2 and 250 keV. A similar analysis is planned which accounts simultaneously for the D(d,n) and D(d,p) reactions. In the meantime, we have generated D-D reaction parameters at temperatures between 0.2 and 250 keV using the cross-section curves contained in Greene's report.<sup>3</sup> The Maxwellian-averaged integrations were performed using the STEEP code.<sup>4</sup> The resulting parameter curves are shown in Fig. 1.

Numerical comparisons of the present results with values tabulated in Ref. 3 show that our reaction parameters for D-T are ~10% higher in the vicinity of 0.2 keV and differ at most by 4% at temperatures between 2 and 250 keV; our reaction parameters for D-<sup>3</sup>He are consistently higher than Greene's, with the difference approaching 20% at 20 keV temperature. The latter difference comes mainly from the fact that the R-matrix calculations predict a <sup>3</sup>He(d,p) cross section that is 15% higher in the resonance peak (at  $E_d = 430$  keV) than that used by Greene.

B. GNASH Code Development (E. D. Arthur and P. G. Young)

The Nuclear Model Codes Subcommittee of the Cross Section Evaluation Working Group (CSEWG) has expressed interest in the testing and evaluation of model codes that can be used in the interpretation of nuclear data. As part of this effort, we were

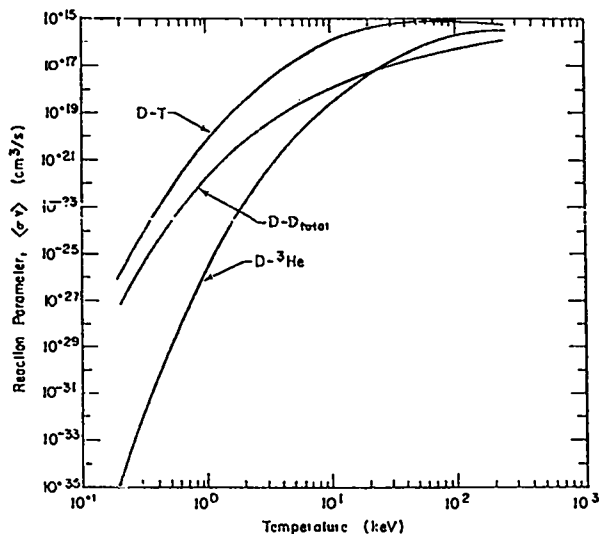


Fig. 1. Maxwellian-averaged thermonuclear reaction parameters for  $T(d,n)^4\text{He}$ ,  $^3\text{He}(d,p)^4\text{He}$ , and the sum  $[D(d,n)^3\text{He} + D(d,p)T]$ .

asked to calculate 14-MeV neutron-induced reactions on Nb, using our newly developed statistical model code GNASH. For this effort, transmission coefficients for neutrons and charged particles were generated with the optical model routines of COMNUC, and were based on the global parameters reported by Perey and Perey.<sup>5</sup> Cross sections and spectra resulting from neutron-induced reactions on Nb were calculated simultaneously, the results of which were sent to other members of the subcommittee.

#### C. Calculation of $(n,xn)$ Cross Sections (E. D. Arthur and L. R. Veaser [P-3])

We have begun calculation of  $(n,2n)$  and  $(n,3n)$  cross sections with the statistical model code GNASH. This effort will provide theoretical results to be compared with experimental  $(n,xn)$  cross sections measured by P-3. As a first step, the  $^{197}\text{Au}(n,3n)$  cross section was calculated along with spectra which included preequilibrium contributions. These results will be used to correct the efficiency of the experimental apparatus used in the measurements.

#### D. Evaluation of $^6\text{Li}$ Neutron Cross Sections Above 1 MeV (L. Stewart, P. G. Young, and V. Stovall)

All cross sections are re-evaluated and in the ENDF/B-IV format. The only cross section identical to that in Version IV is the  $(n,\gamma)$  reaction. (This was completely updated from Version III to IV.) The experimental data for the  $(n,n'd)$  and  $(n,2n)$  cross sections, which are important for weapons applications, are so discrepant among themselves that it is

difficult to assess the reliability of this file above 1 MeV. Unfortunately, both the elastic scattering and the  $(n,t)$  cross sections are also discrepant over a significant portion of the energy range, therefore prohibiting the usual checks by subtraction methods. New total cross-section experimental measurements from Rensselaer Polytechnic Institute (RPI) are as much as 3 to 4% higher over most of the range than previous data from Hanford Engineering Development Laboratory (HEDL).

The most significant improvement in the evaluation is the introduction of "pseudo levels" in the  $(n,n'd)$  reaction in order to represent a reasonable energy-angle correlation for the inelastic neutrons. Although the first excited state in  $^6\text{Li}$  is the only level uniquely identified by experiment, 3-body phase-space calculations have shown reasonable agreement with the measured continuum distributions as a function of angle. Phase-space calculations have been performed and angular distribution data entered in File 4 of this evaluation. In the previous evaluation, no energy-angle correlated data were provided and energy was often not conserved on the average for the  $(n,n'd)$  reaction. The disadvantage in using the pseudo levels is that the file becomes somewhat voluminous. The LR flag will be implemented to enable the processing codes to pick up the  $d + \alpha$  decay which follows the excitation of most levels in  $^6\text{Li}$ .

Complete files in the ENDF/B-IV format should be available to LASL users in September. A reevaluation of the files below 1 MeV should be available this calendar year.

#### E. Evaluation of $^{15}\text{N}$ Neutron Cross Sections (E. D. Arthur, G. M. Hale, and P. G. Young)

Since the thresholds for neutron-induced absorption reactions on  $^{15}\text{N}$  are relatively high, the use of  $^{15}\text{N}$ -enriched fuels is of interest, particularly for fast reactors. We have completed the major part of our evaluation of reactions on  $^{15}\text{N}$  induced by neutrons from  $10^{-11}$  to 20 MeV.

We used an R-matrix analysis to evaluate the  $n + ^{15}\text{N}$  system below 5.4 MeV. We have fitted the available total cross section,<sup>6</sup> angular distributions,<sup>6,7</sup> and polarization data<sup>6</sup> in this energy region. In doing so we have extended the R-matrix analysis of this system to a higher energy region than previously reported.<sup>6</sup>

The experimental data above 6 MeV show little resolved structure in the measured cross sections; therefore, we used a statistical model calculation in the evaluation from 6 to 20 MeV. We calculated cross sections with two model codes. The first of these, GNASH, provided calculated gamma-ray, neutron, and charged-particle spectra. To account for departures from the statistical model due to direct reactions, we included a pre-equilibrium component<sup>8</sup> in the particle spectra calculations. The second code, COMNUC, allowed us to calculate the angular distribution of elastically scattered neutrons. In both codes the Gilbert and Cameron level density approximation was used, along with neutron and charged particle transmission coefficients based on optical-model parameters reported in the global compilation of Perey and Perey.<sup>5</sup>

F. Cross-Section Uncertainty Evaluation for <sup>27</sup>Al  
(D. G. Foster, Jr. and P. G. Young)

Correlated uncertainty information has been obtained for the ENDF/B-IV <sup>27</sup>Al evaluation. Estimates of the diagonal elements of the covariance matrices for the (n,p) and (n,α) reactions were obtained from crude estimates of ± 2σ using all experimental data; for other reactions, a revised version of Table VI in Ref. 9 was used. Correlations were estimated from consideration of the experimental data and theoretical calculations used in the Version IV evaluation. The results of the error analysis are available in ENDF/B format.

G. Time-Dependent Photon Spectra from Fission of <sup>235</sup>U and <sup>239</sup>Pu  
(D. Graham Foster, Jr.)

The evaluation reported last quarter has been revised and extended in order to improve its applicability to a reactor-related problem. The original application called for a compact representation emphasizing rather early times after fission, and hence was arranged to include the "prompt" photons in the ENDF/B-formatted Files 17 and 18. Since this is a violation of the ENDF/B procedures, this feature has been removed, and the zero-time spectrum now corresponds only to the zero-time extrapolation of the delayed emission. This change has the additional advantage that variations in yield and spectrum with incident-neutron energy are already represented in ENDF/B-IV, whereas there is not enough experimental information available to supply such variation for the delayed emission.

In addition, the evaluation has been extended to give yields of delayed photons up to 10<sup>8</sup> s (3.17 yr). The extension is based on an old ORNL measurement by Maienschein et al.<sup>10</sup> supplemented with the radiochemical data of Perkins and King,<sup>11</sup> which was published as the photon power emission as a function of time. Since the spectrum changes very slowly between 1 ms and 60 s, we have assumed that the same spectrum can be used from 60 to 10<sup>8</sup> s, and used the shape of the curve (Refs. 10 and 11) to determine the variation of yield with time. Unfortunately, the ORNL data are tangent to the previous evaluation at 15 s rather than near 60 s, and decrease so much more slowly with time that they imply a yield at 60 s about a factor of 3 higher than was obtained from the Fisher-Engle measurement<sup>12</sup> used in the original evaluation. Thus, the error assigned to the extension beyond 30 s is roughly a factor of 2, rather than the 20% estimated for earlier times after fission. The radiochemical data end at 50 000 s, so the curve is extrapolated to 10<sup>8</sup> s by assuming a straight line on a log-log plot, as suggested by the data between 8000 and 50 000 s.

We expect before the end of FY75 to replace this extension with calculated yields and spectra from ENDF/B-IV data on the fission products.

Since the evaluation effort over the past two quarters represents the first attempt that we know about to use the delayed-emission ENDF formats, we have written proposed sections for the Formats and Procedures Manual covering Files 17 and 18. If these prove acceptable to CSEWG it is hoped that they will be published in time to guide preparation of further files for Version V.

H. Development of ENDF/B Formats for Activation and Decay Data  
(L. Stewart, R. J. LaBauve, and P. G. Young)

At the request of the now inactive CTR Subcommittee of the United States Nuclear Data Committee (USNDC), an action was placed on L. Stewart to design a format for the representation of activation data. Currently, the ENDF/B-IV format does not allow evaluators to indicate whether the end product produced in a neutron reaction is stable or unstable. From the growing interest of LASL designers and Don Steiner's statement that this format is most important to CTR designers, we decided that we should proceed with a format proposal to submit to CSEWG for Version V of ENDF/B.

A preliminary draft has been given a limited distribution which includes several "labels" in the general purpose files; the half-life and mode of decay for each radioactive nuclide produced in each reaction will now appear. In addition, new ENDF files are proposed for activation cross sections or multiplicities for unique identification. All of this information must be correlated with the "decay data" which also has a new format proposal for Version V. So far, no real problems have developed and consensus has been reached in melding these files with the decay data files. A formal proposal will be submitted to CSEWG in August for approval at the October meeting. Comments and corrections on the preliminary draft can be incorporated if received at an early date.

## II. NUCLEAR CROSS-SECTION PROCESSING

Group T-2 is supporting and developing a variety of computed codes for processing evaluated nuclear data into forms that can be used for design purposes. It is also producing processed data sets for various national and LASL programs. The following subsections summarize recent progress.

### A. Cross-Section Production (R. B. Kidman, R. E. MacFarlane, and R. J. Barrett)

The 50-group, 22 isotope library generated with MINX from ENDF/B-IV and distributed to several laboratories last quarter, contained several errors that were uncovered during initial use. New 50-group MINX runs have been made for  $^{238}\text{U}$ ,  $^{239}\text{Pu}$ , and Fe to correct most of these errors. The new results were merged into the 22-isotope library, combined with new versions of the LINX, BINX, and CINC codes and distributed to several laboratories involved in Phase II testing of ENDF/B-IV. A completely new issue of the 50-group library using the pre-release version of MINX will be made available through the National Neutron Cross Section Center (NNCSC) and Brookhaven National Laboratory (BNL).

The latest version of the ENDF/B-IV data has been converted into binary mode and stored in PHOTOSTORE. This data is available to any LASL users using ENDF/B processing codes which accept binary input; it also provides an independent backup for the BCD tapes and BCD PHOTOSTORE files.

### B. MINX Code Development (R. E. MacFarlane, R. M. Boicourt, and R. B. Kidman)

A serious difficulty with the reconstruction of point resonance cross sections was discovered this quarter. The BCD ENDF/B format tapes used for pointwise cross sections in MINX are limited to six significant figures to represent energy points. In narrow resonance materials such as  $^{238}\text{U}$  (ENDF/B-IV MAT 1262), more than six figures are sometimes required to represent the cross section. The RESEND code<sup>13</sup> used for resonance reconstruction in MINX was designed to remove energies that would be equal to an adjoint energy on the BCD tape. This algorithm was faulty and was rejecting too many points. A new truncation algorithm has been installed which includes a message to indicate when energy points have been rejected. The new version of RESEND generates over 50 300 points rather than the previous 33 500 points for a 1% tolerance, and the new error message indicates that the reconstruction still has not completely converged. The multigroup cross sections computed with this new reconstruction technique agree with ETOX (Ref. 14) cross sections to within 1% except for one group which deviates by almost 2%. The 33 500 point tape gave differences up to 6%. An ultimate solution to this problem could be obtained by using a binary interface tape or by modifying RESEND to reconstruct the cross sections at 300°K by "psi-chi" methods. Both proposals are being studied.

The error which led to problems with the inelastic cross sections of  $^{238}\text{U}$  and Fe on the first release of the MINX 50-group library has been discovered and fixed. It occurred when the threshold group required more than one page of data to represent the cross section. The contributions from the lower page were lost, leading to a severe reduction in the cross section.

Two important improvements have been made to the calculation of unresolved, resonance region cross sections: the File 3 background cross sections are now properly included, and a new quadrature scheme<sup>15</sup> has been installed for computing statistical averages. This quadrature set leads to significant improvements in the cross sections as demonstrated by comparisons with analytic cases. The effect of this change on  $k_{\text{eff}}$  for two benchmark critical assemblies is discussed in Sec. III-B.

Preparations for releasing MINX and its auxiliary codes have continued with extensive editing of the code structure and comments, a complete rewrite of the error message system, the addition of the 50-group library structure to the list of group options, and a determined effort to reduce the amount of paper required by the output listing. The code errors in CINX reported last quarter have been corrected. In addition, many changes have been made to LINX, BINX, and CINX to make them more machine independent.

C. NJOY Code Development (R. E. MacFarlane, R. M. Boicourt, W. B. Wilson, and M. L. Simmons [CMB-8])

The development of the NJOY nuclear data processing system (originally MINX-II) has continued this quarter with several small corrections and changes (such as the addition of new group structure and weighting options), and five major additions: blocked binary data transfer, DTF format output, photon transition probability table processing, multigroup covariance matrix processing, and unresolved resonance calculation improvements.

Studies of the NJOY group-averaging module GROUPR using the LASL system utility STAT have shown that the code spends about 60% of its time decoding BCD format statements. For some processing functions this ratio has been seen to reach 80%. It is clear that the use of binary formats to transfer data would lead to a major increase in code efficiency. The NJOY code system was originally designed with binary I/O as a central feature -- this feature has now been activated. A special "blocked binary" version of the ENDF/B format has been developed which allows LIST and TABL records to be divided into blocks or pages of convenient size (for example, 300 words). Even large pointwise data tapes, which may contain TABL records over 100 000 words long, can be represented in binary mode using this method. A set of utility routines was developed to manipulate these data blocks; for example, to read a TABL record page by page, the code calls TABLIO for the first page and MOREIO for the subsequent pages. Blocked binary mode ENDF/B tapes can be produced automatically from BCD source tapes using the program MODER. This module can also write an ENDF/B BCD tape for external communications. Tests of this system demonstrate reductions in processing time by factors from 2 to 4 when a blocked binary tape is used as input to GROUPR.

The DTF discrete ordinates transport code<sup>16</sup> is widely used at LASL. Therefore, the first output module developed for NJOY has been designed to produce cross sections for this code using the output tape from GROUPR. The number of groups, table length, number of edit positions, and number of up-scatter positions are all completely arbitrary as long as the table size does not exceed 30 000 words. Edit quantities can be expressed quite generally as any linear combination of ENDF/B cross sections. Fission yields and spectra are computed from the fission transfer matrices and group fluxes passed by GROUPR. The module also retrieves the photon production cross sections on the GROUPR output tape and sums them into photon production matrices (including anisotropy if desired). These tables are ready to be used for computing gamma sources or for incorporation into coupled sets.

With the addition of processing for the photon transition probability tables from File 12 (option L0=2) and the DTF output module, NJOY has been brought into full capability for photon production cross sections. The L0=2 option is handled by converting such a file into the normal L0=1 yield format, and then processing it with the existing coding. The new option has been tested on sodium (ENDF/B-IV MAT 1156) with the results shown in Fig. 2. The right side of this isometric plot contains 94 gamma groups<sup>17</sup> with energy decreasing toward the rear. The left side uses the LASL 30-group structure with larger energies to the rear.

A capability for processing ENDF/B covariance files is under development for NJOY. The ERRORR routine takes full advantage of the modular nature of NJOY including BCD or binary input and access to preprocessed libraries of group constants. Its capabilities are very similar to those of the pioneering covariance processor, PUFF,<sup>18</sup> except for the following two extensions: (a) internal processing of covariances for cross sections derived by different formulae in different energy ranges, and (b) approximate processing of covariances directly from an existing preprocessed library of group constants in a supergroup structure.

Covariances for derived cross sections are important for all materials. Experimentalists are generally not able to measure a given cross section at all energies; the evaluator may have to compute

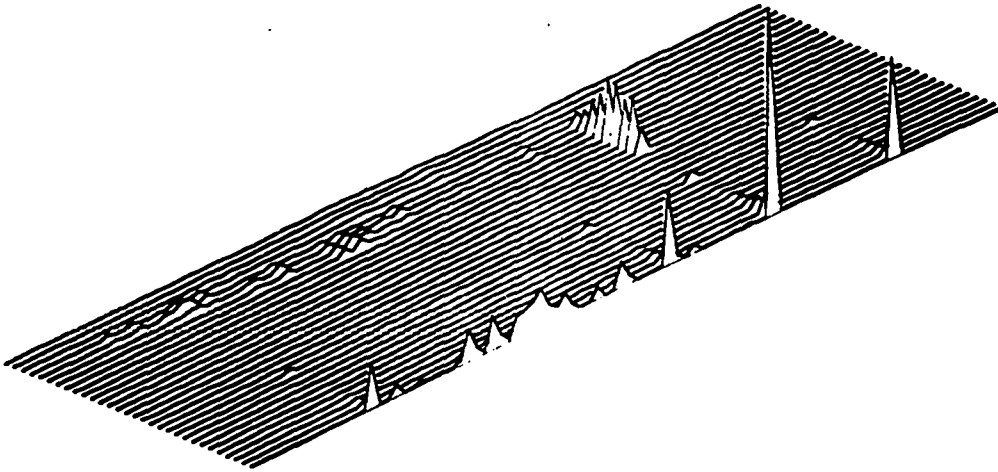


Fig. 2. Photon production cross sections for  $^{23}\text{Na}$ . Photon groups are on the right with energy decreasing to the rear. Neutron energies increase toward the rear.

this cross section from other measured cross sections in some energy ranges. For example, in the new LASL evaluation of errors in aluminum, the elastic scattering cross section is given as total minus capture minus  $(n,n')$  minus  $(n,p)$  for energies less than 9 MeV; it is evaluated directly between 9 and 17 MeV and is expressed as one-half the total cross section from 17 to 20 MeV. In the error evaluation for nitrogen,<sup>19</sup> the total is derived below 1 keV, elastic is derived from 1 keV to 10 MeV, and  $(n,n')$  is derived above 10 MeV. The ENDF/B formats for File 33 allow for flagging cross sections which are derived in a particular energy range -- these flags have been used for carbon and aluminum. If the derived cross-section flags had been available for use with the nitrogen evaluation, they would have saved the evaluator much effort and reduced the size of the file from 599 to 216 cards. The extended capabilities for handling derived cross sections in ERRORR were designed to handle aluminum and modified versions of the nitrogen and oxygen files using the derived cross-section flags. The current version of the code reads the relationships between the cross sections in each energy range as input, but minor changes in formats and procedures for File 33 will allow all processing to be completed automatically.

One of the problems with group-wise covariance matrices is the huge volume of data generated for all but the coarsest group structures. A tendency has developed in recent years to use "supergroup"

structures such as the CSEWG 239 group structure<sup>20</sup> for storage of group constants which are then collapsed to a coarse group structure for actual calculations. If a supergroup library of covariance matrices were generated for nitrogen with 5 reactions, more than 435 000 covariances might have to be stored. Since future evaluations are likely to include even more reactions, this approach seems impractical. The alternative to computing the covariances for each coarse group design structure is time consuming. Since NJOY is organized around the use of preprocessed group constants, an option has been included in ERRORR to use preprocessed group fluxes and cross sections in the calculation of covariances. This option involves some approximation of the energy ranges from the evaluation in File 33. The differences introduced by this approximation are negligible for all existing and anticipated error files.

The implementation of these extensions in the ERRORR module of NJOY plus some minor changes in formats and procedures significantly eases the effort of preparing evaluated error files and makes the preparation of group covariances easier and less costly.

The unresolved resonance region module UNRESR has been extended to include the effects of background cross sections and to use the new quadrature sets for statistical averaging. These changes were similar to those made in MINX (see Sec. II-B) and both codes give the same answers.

A paper summarizing the NJOY code has been accepted for presentation at the 1975 Winter Meeting of the American Nuclear Society.

D. Advanced Processing Theory (R. E. MacFarlane and M. Becker [Rensselaer Polytechnic Institute])

In order to justify the use of existing processing methods and to develop new methods for advanced codes, a long range program of studying the approximations used in the MINX and NJOY processors and the follow-on codes such as SPHINX and LDX (Ref. 21) is being pursued.

One of these approximations was discussed in a paper presented at the 1975 Annual Meeting of the American Nuclear Society.<sup>22</sup> As discussed previously, the MINX/SPHINX system assumes that the self-shielding of elastic removal is the same as for the elastic cross section. This was shown to be a bad approximation for iron. Additional calculations have now been performed for <sup>238</sup>U with the results shown in Table I -- here the approximation being questioned is even worse than for iron. The calculated removal is larger than the approximate removal when there is a resonance at the lower boundary of the group, and smaller otherwise. To determine whether the differences observed in the removal cross section have any effect in realistic problems, the flux in a model of the RPI iron transport experiment<sup>23</sup> was computed using DTF-IV (Ref. 16) and two different cross-section sets generated by NJOY. The results are shown in Fig. 3 for the cross-section set using calculated removal (C) and another set using approximate removal (A). Large differences in flux are evident at the lower energies.

Another important and long-standing problem is the effect of deep minima in the scattering cross section of iron. Calculations using the self-shielding factor method for shielding problems and critical assemblies containing iron have often failed to achieve the accuracy demonstrated for the method in other problems.<sup>23,24</sup>

In the Bondarenko method, the weighting flux is assumed to vary in proportion to  $(\sigma_0 + \sigma_t)^{-1}$ , where  $\sigma_t$  is the total microscopic cross section and the parameter  $\sigma_0$  is used to allow for other materials and heterogeneity. In a very large assembly of pure iron ( $\sigma_0=0$ ) this flux becomes large in the cross section minima thereby leading to small group cross sections. In a finite assembly, the long mean free

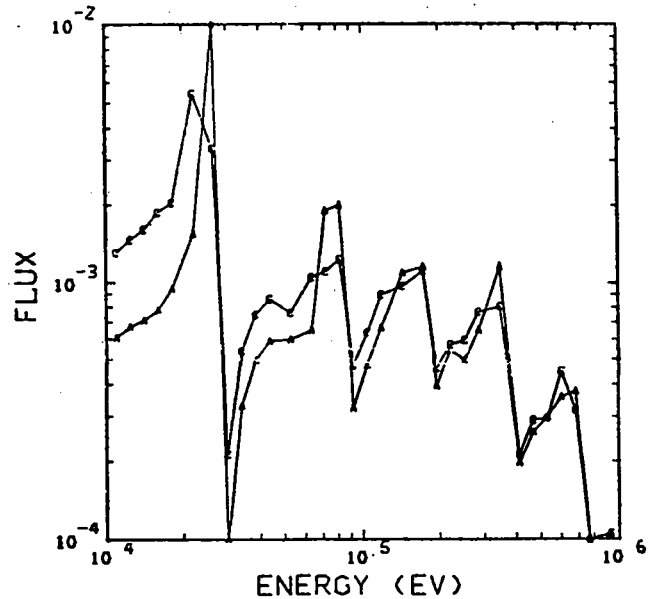


Fig. 3. Neutron flux in the RPI iron transport experiment, using (A) approximate removal cross sections and (C) computed self-shielded removal cross sections.

TABLE I  
COMPARISON OF APPROXIMATE ELASTIC REMOVAL CROSS SECTION WITH COMPUTED SELF-SHIELDED REMOVAL FOR <sup>238</sup>U  
at T=300K,  $\sigma_0=0.1$ , and E<sup>4</sup> WEIGHTING

Group Number*	Calculated Removal	Approximate Bondarenko Removal	Ratio of Results
37	1 57-1	8 31-2	53
38	2 62-2	4 86-3	19
39	1 91-2	1 045	55
40	1 67-2	5 78-3	35
41	2 77-2	3 32-1	12
42	2 72-2	1 12-2	41
43	4 35-2	2 62-3	06

\*49-group structure (Ref. 23)

path of neutrons in these "windows" allows many to escape, thus decreasing the flux in the minimum and increasing the group cross section. This effect can be obtained by (a) choosing an appropriate value of  $\sigma_0$ , (b) flooring the value of  $\sigma_t$  (Ref. 25), or (c) using an entirely different flux shape such as  $(1/b)\tan^{-1}(b/\sigma_t)$  from buckling theory where b parameterizes the leakage.

In order to provide a standard for comparing these three methods, the LASL continuous energy Monte Carlo code MCN (Ref. 26) was modified to compute the elastic scattering cross sections in space and energy cells for a model of the RPI iron trans-

port experiment.<sup>23</sup> Some representative results are compared with the three self-shielding options in Table II.

It is clear from an examination of this table that both the Bondarenko approach and the buckling calculation are capable of representing the space and energy variations of the cross sections for this assembly. The apparent change in buckling with radius is due to the nearly exponential variation of flux with radius in this problem. Thus the leakage current (and  $b$ ) is much higher near the center than at larger radii. The flooring method is not capable of representing this space dependence.

To put these results into practice, it is necessary to estimate the correct value of  $\sigma_0$  or  $b$  for each energy group and spatial region in a problem. A space-energy collapse code like 1DX or SPHINX must then extract the appropriate cross sections from a library and combine them into space-dependent cross sections for use in a neutron transport solution.

A paper summarizing this work has been accepted for presentation at the 1975 Winter Meeting of the American Nuclear Society.<sup>27</sup>

Additional investigations have been initiated on the feasibility of using the method of self-shielding factors in the epi-thermal range important to light water and graphite moderated power reactors. Initial results for High Temperature Gas-Cooled Reactor (HTGR) fuel elements are described in Sec. IV.

### III. PHASE II TESTING OF ENDF/B-IV DATA

#### A. Phase II Results for Benchmark Criticals (R. B. Kidman and R. J. Barrett)

Every new version of ENDF/B data is tested by computing several integral parameters for the various CSEWG benchmark criticals and comparing the results with measured values. We have completed the calculations for four critical assemblies assigned to LASL. Figure 4 shows the procedure and codes used in our calculations. The 50-group cross sections generated with MINX and distributed last quarter were also used here. The eigenvalue results are shown in Table III (no correction factors have been applied). Table IV contains the calculated-to-experiment (C/E) values for the central reaction rate ratios. The 1DX results have been included for the sake of comparison and to obtain 1DX-to-DTF correction factors if they are desired.

TABLE III  
CALCULATED EIGENVALUES<sup>a</sup>

Benchmark	Using 1DX	Using DTF ( $S_{16}$ )
JEZEBEL	0.94781	1.00000
VERA-11A	0.94611	0.99364
GODIVA	0.97468	1.01201
ZPR-3-U	1.01029	

<sup>a</sup>Experimental eigenvalues are equal to 1.0.

TABLE II  
COMPARISON OF SELF-SHIELDING APPROXIMATIONS FOR THE ELASTIC SCATTERING CROSS SECTION OF IRON WITH MONTE CARLO RESULTS

Lower Energy (eV) <sup>a</sup>	Monte Carlo		Bondarenko		Floored	Buckling	
	15 cm	45 cm	$\sigma_0=0b$	$\sigma_0=0.5b$	$\sigma_t=0.5b$	$b=1b$	$b=0.1b$
1.703+4	2.52	2.53	2.53	2.53	2.53	2.53	2.53
1.903	2.03	2.04	2.04	2.04	2.04	2.04	2.04
2.479	6.93	6.99	6.73	7.14	6.72	6.83	6.73
2.809	27.5	27.2	26.3	26.5	26.3	26.4	26.3
3.183	9.39	9.44	9.42	9.44	9.42	9.42	9.42
3.606							
⋮							
1.259+5	2.44	2.10	1.94	2.42	2.05	2.37	1.95
1.616	1.85	1.77	1.72	1.96	1.78	1.94	1.72
1.831	3.72	3.38	3.38	3.92	3.38	3.81	3.39
2.075	2.77	2.60	2.54	2.81	2.56	2.79	2.54
2.352	2.41	2.38	2.37	2.42	2.37	2.41	2.37
2.665	1.94	1.77	1.74	1.98	1.74	1.94	1.75
3.020	1.84	1.54	1.84	1.57	1.57	1.81	1.57
3.877							
⋮							

<sup>a</sup>49-group structure (Ref. 21).

TABLE IV  
CENTRAL SPECTRAL INDICES (C/E)

Ratio	JEZEBEL		VERA-11A		GODIVA		ZPR-3-11	
	1DX	DTF	1DX	DTF	1DX	DTF	1DX	DTF
$\sigma_f(^{238}\text{U})/\sigma_f(^{235}\text{U})$	0.924	0.940	1.095	1.145	1.049	1.068	1.057	1.052
$\sigma_f(^{233}\text{U})/\sigma_f(^{235}\text{U})$	0.930	0.929	0.996	0.996	0.925	0.924	0.998	0.998
$\sigma_f(^{239}\text{Pu})/\sigma_f(^{235}\text{U})$	0.932	0.935	1.074	1.083	0.968	0.970	0.985	1.004
$\sigma_f(^{237}\text{Np})/\sigma_f(^{235}\text{U})$	0.927	0.939	1.131	1.173	--	--	1.056	1.052
$\sigma_f(^{240}\text{Pu})/\sigma_f(^{235}\text{U})$	--	--	1.046	1.082	--	--	1.059	1.056
$\sigma_{n,\gamma}(\text{Au})/\sigma_f(^{235}\text{U})$	--	--	--	--	0.870	0.859	--	--
$\sigma_f(^{234}\text{U})/\sigma_f(^{238}\text{U})$	--	--	--	--	0.911	0.904	--	--
$\sigma_{n,\gamma}(^{238}\text{U})/\sigma_f(^{238}\text{U})$	--	--	--	--	0.958	0.934	--	--
$\sigma_f(^{232}\text{Th})/\sigma_f(^{238}\text{U})$	--	--	--	--	0.989	0.991	--	--
$\sigma_f(^{234}\text{U})/\sigma_f(^{235}\text{U})$	--	--	--	--	--	--	1.045	1.042
$\sigma_f(^{236}\text{U})/\sigma_f(^{235}\text{U})$	--	--	--	--	--	--	0.789	0.786
$\sigma_{n,\gamma}(^{238}\text{U})/\sigma_f(^{235}\text{U})$	--	--	--	--	--	--	0.942	0.962

B. Discrepancies in Phase II Results (R. B. Kidman and R. J. Barrett)

When the Phase II testing results from several laboratories were compared during the May 1975 CSEWG Meeting, several bothersome discrepancies appeared. The  $k_{\text{eff}}$  results for ZPR-6-7 (see Table V) can serve to point out the problems. (Although this benchmark was not assigned to LASL for computation, we have gone ahead and calculated it in order to help resolve the discrepancies.)

The HEDL and Brookhaven National Laboratory (BNL) results should have been the same since they used the same cross sections and methods. However this discrepancy could be due to the fact that BNL's version of 1DX may be using an old interpolation scheme.

Since SPHINX and 1DX are nearly the same, one would think the Westinghouse Advanced Reactor Division (WARD) and LASL results could be closer. One reason for the discrepancy is that WARD and LASL used different fission sources which we have found accounts for 0.00125 of the discrepancy. Gene Paik of WARD has also informed us that the different elastic down-scattering treatments in SPHINX and 1DX account for an additional 0.0025 of the discrepancy. This leaves only a 0.25% difference between the WARD and LASL numbers.

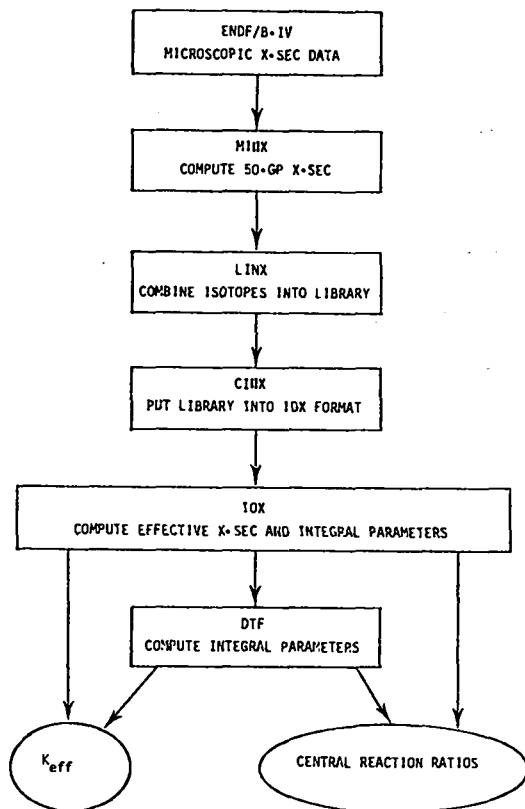


Fig. 4. Calculational procedure.

Finally, even though the methods are different, the Argonne National Laboratory (ANL) results should be closer to the LASL or HEDL results since they are all calculating the same reactor. Again we have found that the use of different fission sources can explain 0.0025 of the difference. H. Henryson of ANL has informed us of an improved method (that MC<sup>2</sup> uses) of computing averages with a Porter-Thomas distribution weighting function. We have thoroughly tested the effects of this change by generating a complete isotope library for each of the methods and using IDX to calculate ZPR-6-7 with each library. It turns out the new ANL method gives a lower k<sub>eff</sub> by 0.0043; hence there only remains a 0.04% difference between the ANL and LASL results. In summary, if the above known differences are removed, the eigenvalue for ZPR-6-7 should be closer to the numbers in parentheses in Table V.

C. GODIVA and JEZEBEL 26-Group Transport Calculations (R. J. LaBauve and W. B. Wilson)

In conjunction with the CSEWG data testing program, 26-group cross section sets have been produced by MINX<sup>28</sup> for GODIVA and JEZEBEL calculations. Using the one-dimensional neutron transport code DTF-IV,<sup>16</sup> spectral indices and eigenvalues were calculated with a variety of calculational parameters.

Separate transport calculations were performed with P<sub>0</sub> through P<sub>5</sub> truncated and P<sub>0</sub> through P<sub>4</sub> transport-corrected<sup>29</sup> cross-section sets using S<sub>16</sub> quadrature. Additional P<sub>5</sub> calculations were made with S<sub>8</sub> and S<sub>4</sub> quadrature.

Spectral indices and eigenvalues calculated with S<sub>16</sub> quadrature were found to oscillate but converge as the number of cross-section tables used increases, with P<sub>n</sub> transport-corrected cross sections yielding values intermediate to those calculated with P<sub>n</sub> and P<sub>n+1</sub> truncated cross sections below P<sub>4</sub>. An eigenvalue correction of -0.003 was estimated for P<sub>0</sub> transport corrected to P<sub>∞</sub> for both JEZEBEL and GODIVA.

Values calculated with different quadratures converge slowly but monotonically as the number of quadrature angles increases.

IV. NUCLEAR DATA PROCESSING FOR HTGR SAFETY RESEARCH (M. G. Stamatelatos, R. J. LaBauve, and K. Hansborough)

LASL cross sections for 300, 1200, and 3000°K were discussed in the previous progress report. The major source of disagreement with General Atomics (GA)

TABLE V  
k<sub>eff</sub> RESULTS FOR ZPR-6-7

Laboratory	k <sub>eff</sub>	After Differences Are Removed
ANL (MC <sup>2</sup> )	0.967	(0.9695)
HEDL (ETOX-1DX)	0.9754	(0.9699)
WARD (MINX-SPHINK)	0.968	(0.9675)
LASL (MINX-1DX)	0.9734	(0.9691)
BNL (ETOX-1DX)	0.973	(0.9699)

cross sections was found in the resolved resonance region where, in the case of the capture cross section of <sup>232</sup>Th, the MC<sup>2</sup> (Ref. 30) homogenized cross section was found to be lower than the GA cross section in which spatial heterogeneities had been accounted for. This discrepancy was initially attributed to a possible coarse energy-mesh representation in MC<sup>2</sup> for the resonance region.

"Ultra-fine" MC<sup>2</sup> runs performed with ~2000 energy groups (1/120 equal lethargy mesh) between 10 MeV and 0.414 eV at 300 and 3000°K have revealed negligible differences from the corresponding "all-fine" MC<sup>2</sup> results using 68 equal lethargy (0.25) groups for the same energy range.

The 68 fine-group MC<sup>2</sup> capture cross sections were then compared with MINX<sup>28</sup> cross sections generated in the same GAM-I energy structure. The general agreement between these two sets has indicated that the MC<sup>2</sup> fine-group capture cross sections were not the main cause of discrepancy between the MC<sup>2</sup> and the GA broad-group capture cross sections. The broad-group collapsing method in MC<sup>2</sup> became immediately subject to inquiry.

Briefly, the MC<sup>2</sup> multigroup averaging method for the resolved-resonance capture cross section is as follows:

$$\left(\frac{-bg}{\sigma_c^J}\right)_{resolved} = \frac{\sum_{j \text{ in } J} \langle \sigma_c \rangle_j^{fg} \text{ resolved } Q_j}{\sum_{j \text{ in } J} Q_j} \quad (1)$$

where

$$Q_j \equiv \int_{E_j}^{E_{j+1}} S_j^{fg} \frac{dE}{\Sigma_T(E)} \quad (2)$$

and

$$\begin{aligned}
s_j^{fg} = & \sum_{k \neq j} \Sigma_{inel,k}^{fg} \phi_k^{fg} \frac{\langle \Sigma_{inel}^{k \rightarrow j} \rangle}{\langle \Sigma_{inel}^k \rangle} \\
& + \sum_{k \neq j} \Sigma_{n,2n,k}^{fg} \phi_k^{fg} \frac{2 \langle \Sigma_{n,2n}^{k \rightarrow j} \rangle}{\langle \Sigma_{n,2n}^k \rangle} \\
& + \langle \Sigma_{el} \rangle_{j-1 \rightarrow j} \phi_{j-1}^{fg} \quad , \quad (3)
\end{aligned}$$

where superscripts fg and bg indicate broad-group and fine-group, respectively. J and j are subscripts referring to broad-group and fine-group, respectively.

This method of multigrouping was not satisfactorily shown to be valid for thermal reactor systems.

Hand calculations using a straight spectrum weighting method have yielded results in general agreement with the GA broad-group capture cross section. A larger value of the MC<sup>2</sup> resolved-resonance capture cross section was expected since spatial heterogeneity effects were not yet included in the MC<sup>2</sup> calculations.

The straight spectrum weighting method was incorporated into MC<sup>2</sup> as an alternative and the subsequent results for 300, 1200, and 3000°K were in reasonable agreement with the GA cross sections.

In order to properly account for the double heterogeneity effects on cross sections as well as to take full advantage of the most up-to-date computational techniques employed in the MINX code system, the following course of action has been adopted:

1. Use MINX for generating point-wise cross sections in ENDF/B format (PENDF) over the entire energy range desired and for all materials of interest.
2. Apply particle heterogeneity corrections to the point-wise cross sections in both the above-thermal (resonances) and thermal regions.
3. Use MINX to collapse the particle-heterogeneity corrected PENDF cross sections to the desired fine-group energy structure.
4. Calculate a fine-group neutron spectrum in the above-thermal region with the 1DX code<sup>21</sup> and use the same code to collapse the above-thermal fine-group cross sections applying the proper "gross" (fuel-pin/moderator) heterogeneity correction for HTGR fuel pins in a hexagonal lattice. The

1DX code has been adapted to accept fine-group cross sections from MINX in the Bondarenko formalism.

5. Collapse the thermal fine-group cross sections with the GLEN code.<sup>31</sup>
6. Investigate the importance of gross heterogeneity effects on thermal cross sections.
7. Format final broad-group cross sections for input to the DTF-IV discrete-ordinates transport code.<sup>16</sup>

The initial procedure in applying the particle heterogeneity corrections to the PENDF capture cross sections is the Sauer formalism used by Wälti in the MICROX code.<sup>32</sup> Preliminary results for the two important capture resonances in <sup>232</sup>Th, at 21.78 and 23.45 eV, have shown flux "disadvantage factors" for 400-micron ThC<sub>2</sub> particles of ~0.7 and 0.58, respectively, in good agreement with Wälti's results.<sup>33</sup> Calculations for ThO<sub>2</sub> particles are in progress.

Comparisons of Wälti's method for treating particle heterogeneity effects on cross sections with other compatible methods, and possibly Monte Carlo calculations, are also anticipated.

## V. NUCLEAR DATA FOR CTR APPLICATIONS

### A. Evaluation of Cross-Section Uncertainties for TFTR Data Assessment (V. Orphan [Science Applications], D. W. Muir, and D. G. Foster, Jr.)

In this quarter, some work has been done in the construction of formatted error files for ENDF/B (notably aluminum). However, the emphasis has been placed on obtaining from other sources error information of potential importance in the nuclear design of the Tokamak Fusion Test Reactor (TFTR). The number of potentially important reactions is very large so that only the broad features of the uncertainty patterns have been represented. Reactions examined so far are listed in Table VI.

### B. Error Processing (D. W. Muir)

To be useful in quantitative data assessment, cross-section error estimates must be processed from continuous-energy representations into multigroup form. Depending on whether the original data is obtained from ENDF/B or from the local estimates described above, one of two different processing techniques has been used.

The processing of ENDF/B formatted error files is accomplished with the PUFF code.<sup>18</sup> This code con-

TABLE VI  
REACTIONS SELECTED FOR  
ESTIMATION OF UNCERTAINTIES

$^{12}\text{C}(n, n'\alpha)^8\text{Be}$	$^{56}\text{Fe}(n, p)^{56}\text{Mn}$
$^{24}\text{Mg}(n, p)^{24}\text{Na}$	$^{58}\text{Ni}(n, p)^{58}\text{Co}$
$^{27}\text{Al}(n, p)^{27}\text{Mg}$	$\text{nat}^{\text{Cu}}(n, \text{total})$
$^{27}\text{Al}(n, \alpha)^{24}\text{Na}$	$\text{nat}^{\text{Cu}}(n, \text{elastic})$
$^{46}\text{Ti}(n, p)^{46}\text{Sc}$	$\text{nat}^{\text{Cu}}(n, \text{inelastic})$
$^{48}\text{Ti}(n, p)^{48}\text{Sc}$	$\text{nat}^{\text{Cu}}(n, \text{absorption})$
$^{52}\text{Cr}(n, 2n)^{51}\text{Cr}(n, 2n)$	$\text{nat}^{\text{Cu}}(n, 2n)$
$^{55}\text{Mn}(n, 2n)^{54}\text{Mn}$	$^{63}\text{Cu}(n, 2n)^{62}\text{Cu}$
$^{55}\text{Mn}(n, \gamma)^{56}\text{Mn}$	$^{63}\text{Cu}(n, \gamma)^{64}\text{Cu}$
$\text{nat}^{\text{Fe}}(n, \text{total})$	$^{63}\text{Cu}(n, \alpha)^{60}\text{Co}$
$\text{nat}^{\text{Fe}}(n, \text{elastic})$	$^{65}\text{Cu}(n, 2n)^{64}\text{Cu}$
$\text{nat}^{\text{Fe}}(n, \text{inelastic})$	$^{65}\text{Cu}(n, \gamma)^{66}\text{Cu}$
$\text{nat}^{\text{Fe}}(n, \text{absorption})$	$^{65}\text{Cu}(n, p)^{65}\text{Ni}$
$\text{nat}^{\text{Fe}}(n, 2n)$	$^{204}\text{Pb}(n, 2n)^{203}\text{Pb}$
$^{54}\text{Fe}(n, p)^{54}\text{Mn}$	$^{206}\text{Pb}(n, \alpha)^{203}\text{Hg}$

sists of an error-processing module developed by ORNL and added to the MINX<sup>28</sup> cross-section processing code, which was developed at LASL. During this fiscal year the combined code was obtained from ORNL and converted from IBM to CDC operation for use at LASL. We have successfully executed a 22-group test problem on  $^{16}\text{O}$  (ENDF/B MAT 1276), which was supplied with the PUFF code. Additional calculations are planned on the ENDF/B error files for carbon, oxygen, and aluminum.

In order to process local estimates of cross section errors and correlations into the form of multigroup covariance matrices, a short program COVMAT has been written. This code interpolates between the input values of cross-section errors and correlation ranges<sup>34</sup> and constructs a full (group-to-group) covariance matrix for the nuclear reaction of interest. Multigroup covariance matrices have been generated using COVMAT for all of the reactions listed in Table VI. The energy-group structure consists of 20 equal-lethargy groups spanning the range from 2.02 to 14.92 MeV.

## VI. DATA ADJUSTMENT METHODS

### A. Techniques for Simultaneous Adjustment of Large Nuclear Data Libraries (W. A. Reupke [Georgia Institute of Tech.], D. R. Harris, and D. W. Muir)

In a previous note,<sup>35</sup> techniques for the simultaneous adjustment of large nuclear data libraries were discussed and a method for the adjustment of

arbitrarily large libraries was programmed as an option for the data consistency and sensitivity code ALVIN.<sup>36</sup> This method is applicable only when the basic nuclear data can be assumed to be uncorrelated.

As part of a continuing program of review and evaluation of data adjustment techniques,<sup>37,38</sup> this restriction has now been relaxed by assuming that only the differential data are not correlated with the integral data. Thus, correlations between individual differential data as well as between individual integral data are allowed in the present technique. As before, the matrix inversion requirements are reduced by expressing the adjustments of the differential data in terms of the adjustments to the integral data (which are usually less numerous). The mathematical background of this approach is summarized in a compact matrix formulation in Sec. VI-B.

This more general technique has been programmed as a new option in the ALVIN code, which is being applied to the analysis of differential and integral neutronic data of importance in the fission and fusion energy regions.

### B. Matrix Formulation of Data Adjustment Methods (W. A. Reupke [Georgia Institute of Technology])

The data adjustment technique mentioned in the previous section is formulated here in a compact matrix notation developed in a critical review of data adjustment methods.

Consider the linear model

$$O(AX) = AX + \epsilon \quad , \quad (4)$$

where the vector  $O(AX)$  represents an observation of the linear function  $AX$  defined on the parameter vector  $X$  and perturbed by random errors  $\epsilon$ . (All symbols denote matrices unless otherwise noted.) The errors are sampled from a multivariate probability distribution with finite second moments and zero means. The observations,  $O(AX)$ , and an initial estimate of the dispersion matrix for these data,  $D[O(AX)]$ , form the primary input data for these data adjustment methods. As shown below, the matrix  $D[O(AX)]$  need only be estimated to within a scalar factor  $s^2$ , since this factor is adjusted on the basis of consistency requirements. When the number of elements  $L$  in  $O(AX)$  exceeds the number of elements  $N$  in  $X$ , i.e., the  $L \times N$  matrix  $A$  satisfies  $L \geq N$ , then mini-

mum variance, unbiased estimates of X and of AX are given by the well-known formula

$$\left\{ A^T D^{-1} [O(AX)] A \right\} \hat{X} = A^T D^{-1} [O(AX)] O(AX) \quad , \quad (5)$$

and

$$\hat{O}(AX) = A \hat{X} \quad , \quad (6)$$

where T denotes the matrix transpose operator.

Further, unbiased estimates of the dispersion matrices of X and of O(AX) are given by

$$\hat{D}(\hat{X}) = \hat{s}^2 \left\{ A^T D^{-1} [O(AX)] A \right\}^{-1} \quad , \quad (7)$$

and

$$\hat{D}[\hat{O}(AX)] = A \hat{D}(\hat{X}) A^T \quad , \quad (8)$$

where

$$\hat{s}^2 = \frac{1}{L-N} [\hat{O}(AX) - O(AX)]^T D^{-1} [O(AX)] [\hat{O}(AX) - O(AX)] \quad . \quad (9)$$

Here  $\hat{s}^2$  is an unbiased estimate of the "renormalization factor"  $s^2$ . The variance in the estimate  $\hat{s}^2$  is given by

$$\text{var } \hat{s}^2 = \frac{\hat{s}^2}{2(L-N)} \quad . \quad (10)$$

Here the inversion of matrices of order L x L is required.

In the special case that the observation vector O(AX) is a partitioned vector of N + M elements consisting of an N-element subvector O(X) of "direct" observations (differential data) on X and an M-element subvector O(SX) of "indirect" observations (integral data) on X, Eq. (4) may be written

$$\begin{bmatrix} O(X) \\ O(SX) \end{bmatrix} = \begin{bmatrix} I \\ S \end{bmatrix} X + \epsilon \quad . \quad (11)$$

If it is further supposed that each direct observation is independent of each indirect observation, then we may write

$$D[O(AX)] = \begin{bmatrix} D[O(X)] & 0 \\ 0 & D[O(SX)] \end{bmatrix} \quad . \quad (12)$$

When Eqs. (11) and (12) are inserted into Eqs. (5)-(10), one obtains in a straightforward manner the partitioned forms of the data adjustment relations

$$\left\{ D^{-1} [O(X)] + S^T D^{-1} [O(SX)] S \right\} \hat{X} = D^{-1} [O(X)] + S^T D^{-1} [O(SX)] O(SX) \quad , \quad (13)$$

$$\begin{bmatrix} \hat{O}(X) \\ \hat{O}(SX) \end{bmatrix} = \begin{bmatrix} \hat{X} \\ S \hat{X} \end{bmatrix} \quad , \quad (14)$$

$$\hat{D}(\hat{X}) = \hat{s}^2 \left\{ D^{-1} O(X) + S^T D^{-1} [O(SX)] S \right\}^{-1} \quad , \quad (15)$$

$$\hat{D} \begin{bmatrix} \hat{O}(X) \\ \hat{O}(SX) \end{bmatrix} = \begin{bmatrix} \hat{D}(\hat{X}) & \hat{D}(\hat{X}) S^T \\ S \hat{D}(\hat{X}) & S \hat{D}(\hat{X}) S^T \end{bmatrix} \quad , \quad (16)$$

$$\hat{s}^2 = \frac{1}{M} \left\{ [\hat{O}(X) - O(X)]^T D^{-1} [O(X)] [\hat{O}(X) - O(X)] + [\hat{O}(SX) - O(SX)]^T D^{-1} [O(SX)] [\hat{O}(SX) - O(SX)] \right\} \quad , \quad (17)$$

and

$$\text{var } \hat{s}^2 = \frac{\hat{s}^2}{2M} \quad . \quad (18)$$

The virtue of Eqs. (13)-(18) in this special case is that the inversion of matrices of order L required by the general Eqs. (5)-(10) is replaced by the easier inversion of matrices of order M and N.

A further economy in the matrix inversion<sup>37,38</sup> is possible if the number of direct observations exceeds the number of indirect observations, i.e., when M > N. The general approach is to use  $\hat{O}(SX) = S \hat{X}$  [from Eq. (14)] to transform the N x N system of Eq. (13) into an intermediate M x M system in O(SX),

$$O(SX) - S O(X) =$$

$$- \left\{ S [D O(X)] S^T + D [O(SX)] \right\} D^{-1} [O(SX)] \left\{ \hat{O}(SX) - O(SX) \right\} \quad , \quad (19)$$

and to reexpress Eq. (19) in terms of  $\hat{X}$ ,

$$\hat{X} = O(X) + D [O(X)] S^T G [O(SX) - S O(X)] \quad , \quad (20)$$

where

$$G = \left\{ SD[O(X)]S^T + D[O(SX)] \right\}^{-1}$$

(Note that G is of order M x M only.) As before,

$$\begin{bmatrix} \hat{O}(X) \\ \hat{O}(SX) \end{bmatrix} = \begin{bmatrix} \hat{X} \\ \hat{SX} \end{bmatrix}, \quad (21)$$

but after use of Eq. (20), the analog of Eq. (15) becomes

$$\hat{D}(\hat{X}) = s^2 \left\{ D[O(X)] - D[O(X)]S^T GSD[O(X)] \right\}, \quad (22)$$

and as before

$$\hat{D} \begin{bmatrix} \hat{O}(X) \\ \hat{O}(SX) \end{bmatrix} = \begin{bmatrix} \hat{D}(\hat{X}) & \hat{D}(\hat{X})S^T \\ S\hat{D}(\hat{X}) & S\hat{D}(\hat{X})S^T \end{bmatrix}, \quad (23)$$

where

$$s^2 = \frac{1}{M} \left\{ [O(SX) - SO(X)]^T G [O(SX) - SO(X)] \right\}, \quad (24)$$

and again

$$\text{var } s^2 = \frac{s^2}{2M}. \quad (25)$$

Eqs. (20)-(25) require inversion of matrices only of order equal to the number of indirect observations.

## VII. FISSION-PRODUCT YIELD AND RADIOACTIVE DECAY STUDIES

### A. CINDER Code Development (T. R. England and N. L. Whittemore)

1. Roundoff Criteria (Version 7)<sup>39</sup> The code algorithms have been improved and tested for several extreme variations of irradiation times, cooling times, and chain systematics. The code now handles nuclides in chains having identical destruction rates (hence can treat cyclic chains) and has been validated for irradiation and cooling time increments varying from  $4 \times 10^{-17}$  s to 10 000 h, where the nuclides in each chain had half-lives varying from the microsecond region to infinity. These improvements, along with the original algorithms, ensure accurate calculations of time-dependent nuclide densities and associated quantities (dose, absorption, decay heating, etc.) for the combinations

of irradiation histories and nuclide parameters encountered in such diverse studies as fission bursts, reactor build-up and depletion calculations, and waste management. Unlike other comparable nuclide codes, there is no resort to approximate solutions which apply only to special cases, such as asymptotic solutions for short lived nuclides or assumptions of instantaneous decay. The roundoff algorithms make use of a number related to the word length used on the user's particular computer. If this word length differs from the default value, it can be entered on a data card.

The changes are now being coded into Version 10. An addendum to Ref. 39 describing the criteria has been prepared.

2. Absorption Library (Version 7). A library of chain data adequate for computing the absorption build-up of fission products in any contemporary Light Water Reactor (LWR) has been tested. These non-ENDF/B-IV data have been favorably compared to recently published long-term irradiation experiments and will be used as a reference data set for testing absorption calculations using ENDF/B-IV data during FY76. This reference library agrees with experimental data on total absorption rates within about 5%, which is well within the experimental uncertainty.

### 3. Version 10 Coding and ENDF/B-IV Libraries

The basic functions of Version 10 have been debugged and extensive ENDF/B-IV data libraries are about 70% complete. (Special ENDF/B-IV libraries for Version 7 for gamma-ray spectra calculations and gaseous products are already in use.) Several routines still have to be added to Version 10, but the more basic functions used in calculating nuclide densities, absorption, and decay energies are operational.

Data libraries for Version 10 are being developed at LASL; the code revisions are a joint, informal LASL and Bettis Atomic Power Laboratory (BAPL) effort with some auxiliary work at Knolls Atomic Power Laboratory (KAPL) directed at chain generation directly from ENDF/B-IV files.

### B. ENDF/B-IV Data (T. R. England and R. E. Schenter [Hanford Engineering Development Lab])

Preliminary calculations of decay heating, gamma-ray spectra, delayed neutrons, decay data uncertainties, and other related quantities were reported in an invited paper<sup>40</sup> presented at the 1975 Annual Meeting of the American Nuclear Society.

C. Energy Release from Gaseous and Solid Fission Products Following  $^{235}\text{U}$  and  $^{239}\text{Pu}$  Fission Bursts (T. R. England, R. E. Schenter [Hanford Engineering Development Lab], P. G. Young and N. L. Whittemore)

The energy release from fission products as a function of time following nuclear bursts must be known to properly assess a variety of tactical battlefield situations. The ENDF/B-IV compilation of fission-product yield, cross section, and decay data allows more accurate estimates of fission-product energy release than previously possible. In addition, earlier studies used estimates of energy release from all fission products, without delineation of gaseous and nongaseous components. Because gases that are released in radioactive fallout will have a different spatial distribution than solids, it is important to estimate the magnitude of this effect. We have also extended the cooling range of earlier studies using updated data.

We have calculated the  $\beta$  and  $\gamma$  energy release as a function of time after fast fission of  $^{235}\text{U}$  and  $^{239}\text{Pu}$  for both gaseous fission products and for the total conglomerate of products. The CINDER<sup>39</sup> and RIBD<sup>41</sup> codes were used with the latest ENDF/B-IV fission product data for the calculations. Preliminary values based on a 1 s "burst" and extending from 1 s to 8.1 days were reported last quarter. The recent calculations are based on an infinitesimally short burst and cover the same time range. Gases are assumed to be the unstable isotopes of Br, Kr, I, and Xe, whether formed directly in fission reactions or as radioactive daughter nuclei. The total decay power calculation involves some 712 nuclides; 150 of these are precursors to ~80 gaseous nuclides which were coupled in 61 linear chains for the gas calculation.

Detailed results of these calculations are tabulated in a report.<sup>42</sup> Figure 5 shows a comparison between our results and a commonly used earlier evaluation<sup>43</sup> for the total gamma-ray energy release from all fission products beginning at 10 s. The earlier study was based on more limited fission yield and decay data so the large differences are not surprising. Our results are higher than the earlier ones by about 600% at 10 s and about 30% near 1 h.

The number density and gamma-ray energy release from gaseous fission products are plotted in Fig. 6 as functions of time, following fission of

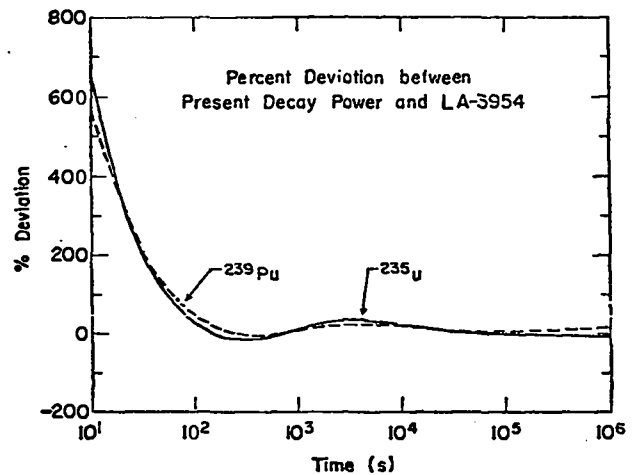


Fig. 5. Comparison of the gamma-ray energy release from all fission products calculated here with that of Ref. 43.

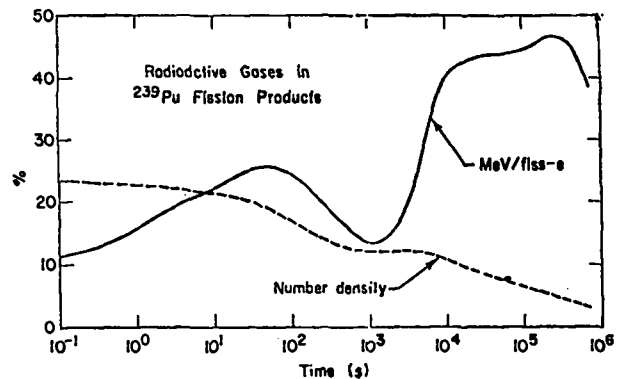


Fig. 6. Percentages of the total number of nuclei produced and gamma-ray energy release that are attributed to gaseous products.

$^{239}\text{Pu}$ . While the relative number of gaseous nuclides formed is not large (less than 25% at all times), the energy release becomes important at times greater than 1 h and approaches 50% of the total gamma-ray energy at times near 1 day. An integral of the energy release for the important time period 0.1 to 50 h shows that about 30% of the gamma-ray energy released in that time region is from gaseous products. While other factors such as gas entrapment and decay of solid daughters from gaseous precursors need to be considered, the present results show that substantial amounts of energy are produced by decay of volatile fission products.

D. Fission-Product Gamma and Photoneutron Spectra and Energy-Integrated Time-Dependent Distributions (M. G. Stamatelatos, T. R. England, and N. L. Whittemore)

Fission-product gamma-ray spectra were calculated with the CINDER-7 code<sup>39</sup> for the ten fission sets ( $^{232}\text{Th}$  fast,  $^{233}\text{U}$  thermal,  $^{235}\text{U}$  thermal,  $^{235}\text{U}$

fast,  $^{235}\text{U}$ -14 MeV,  $^{238}\text{U}$  fast,  $^{238}\text{U}$ -14 MeV,  $^{239}\text{Pu}$  thermal,  $^{239}\text{Pu}$  fast, and  $^{241}\text{Pu}$  thermal), for four irradiation periods (1 h, 1 day, 1 month, and 1 yr) at 50 Watts/cm<sup>3</sup> constant power density ( $\phi_{\text{th}} = 10^{13}$  n/cm<sup>2</sup>/s) and for thirty shutdown time-steps from 1 to 5000 h. ENDF/B-IV data were used including only half-lives in excess of about 15 min and gamma energies in excess of the  $^9\text{Be}$  photoneutron threshold, 1.67 MeV.

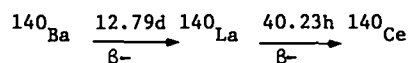
These gamma spectra were used as input to the PHONEX code<sup>44</sup> for calculating photoneutron spectra in  $^9\text{Be}$  and  $^2\text{H}$ . The photon spectra input to PHONEX were not modified to include the effects of scattering or absorption, but these effects have been shown (Ref. 45) to be small.

The gamma and photoneutron spectra were further energy-integrated to obtain total-intensity time-dependent distributions. These intensities were least-squares fitted with sums of minimum numbers of exponentials necessary for an overall fitting to better than 3% between 1 and 500 h after shutdown.

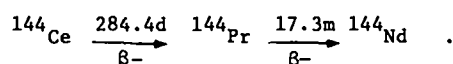
The gamma-ray spectra were calculated in 66 equal energy groups (50 keV grid) and the photoneutron spectra in correspondingly compatible equal-energy groups depending on the threshold energies of the photoneutron reactions.

The main contributors to the relatively high-energy gamma spectra are 32 nuclides, each emitting on the average 16 gamma lines above 1.67 MeV. (One of them,  $^{144}\text{La}$ , has 68 resolved energies about 1.67 MeV.) The concentrations and effective half-lives of these 32 nuclides are significantly affected by 25 precursors. All 57 nuclides are formed in 29 chains. Runs of the CINDER code with and without the inclusion of neutron radiative capture cross sections were performed. The spectral results were found to be very insignificantly affected by the presence of these cross sections in the CINDER calculations.

At large shutdown times, the two most important abbreviated fission-product chains are



and



The direct fission yields of both  $^{140}\text{La}$  and  $^{144}\text{Pr}$  are small so that the decay rate of these hard gammas follow very closely the decay rate of their relatively long-lived precursors. Consequently, the gamma spectra harden with shutdown time between about 10 and 1000 h and the corresponding energy-integrated time distribution remains reasonably flat over approximately the same time interval.

The energy-integrated time distribution can be considered to be the result of the superposition of essentially three distributions. One is a rapidly decaying component due to short-lived daughters having short-lived precursors. The second component, discussed earlier, is due to short-lived daughters with low direct fission yields whose parents are long lived and have significant direct yields. This component rises reasonably fast with irradiation and shutdown time to a level of transient parent-daughter equilibrium concentration whose magnitude is markedly dependent on irradiation periods which are short compared to the precursors' half-lives. The third component, which rises rapidly to a maximum following shutdown and then decays quite rapidly, is due to long-lived daughters with no significant direct fission yields whose parents are shorter lived and have considerable direct yields. This component is essentially independent of the irradiation period prior to shutdown. Its effect on the total time distribution is more visible for short irradiation times causing the total curve to rise slightly between 40 and 100 h and becomes lost in the tail of the slowly decaying transient-equilibrium component for long irradiation times. That is, depending on the irradiation time, these three components can actually combine to cause an increase in the net gamma-ray intensity for a time interval following shutdown.

The most important isotopes contributing to the total curve are shown in Table VII at various shutdown times. They are listed in order of decreasing importance. Gamma spectra and energy-integrated time distributions illustrating the discussed features are shown in Figs. 7-14.

The photoneutron spectra and energy-integrated time distributions follow to a great extent the corresponding gamma distributions (Figs. 15-18). One marked difference is the average photoneutron energy which decreases from 1 to about 10 h shutdown after which it remains essentially constant with shutdown

time (see Fig. 19). By comparison, the average gamma energy decreases from 1 to about 10 h shutdown, then increases considerably to about 1000 h after which it again decreases. Typical results are shown in Fig. 20.

Gamma and photoneutron energy-integrated time-dependent distributions were least-squares fitted, for user convenience, with sums of 3-6 exponentials for the different fission sets and different irradiation periods (see Table VIII). Although the fits are empirical, the importance of  $^{140}\text{La}$  at large shutdown times also becomes evident through the consistent appearance of a fitting exponential term with a decay constant,  $\lambda$ , in the neighborhood of  $2.2576 \times 10^{-3} \text{h}^{-1}$  which is the decay constant of  $^{140}\text{La}$ . The appearance of exponentials with negative coefficients for time distributions corresponding to short irradiation periods is explained by the important contribution in the ~40 to 100 h after shutdown region of chains with long-lived isotopes having short-lived precursors as discussed above.

Because of the near constant or even increasing source strength after ~10 h of cooling, and because of the time-dependent behavior of the average gamma and photoneutron energies, users have requested calculations extending in both the irradiation and the cooling periods. A report on all input data and calculational results is in preparation. Some limited<sup>46,47</sup> interim results have already been published.

TABLE VII  
MAJOR CONTRIBUTORS TO PEAKS IN GAMMA SPECTRA  
( $^{235}\text{U}$  THERMAL FISSION)

ENERGY BIN (MeV)	NUCLIDE(S)
--1 HOURS COOLING--	
1.67-1.75	$^{135}\text{I}$ , $^{98}\text{Nb}$ , $^{134}\text{I}$
1.75-1.80	$^{135}\text{I}$ , $^{142}\text{La}$ , $^{97}\text{Zr}$
1.80-1.85	$^{88}\text{Rb}$ , $^{134}\text{I}$
1.90-1.95	$^{142}\text{La}$ , $^{93}\text{Y}$ , $^{132}\text{I}$ , $^{135}\text{I}$
2.00-2.05	$^{88}\text{Kr}$ , $^{142}\text{La}$
2.15-2.20	$^{88}\text{Kr}$ , $^{142}\text{La}$ , $^{89}\text{Rb}$
2.20-2.25	$^{138}\text{Cs}$ , $^{88}\text{Kr}$
2.35-2.40	$^{88}\text{Kr}$ , $^{142}\text{La}$
2.50-2.55	$^{142}\text{La}$ , $^{140}\text{La}$
--10 HOURS COOLING--	
1.67-1.75	$^{135}\text{I}$
1.75-1.80	$^{135}\text{I}$ , $^{97}\text{Zr}$
1.80-1.85	$^{88}\text{Rb}$ , $^{135}\text{I}$
1.90-1.95	$^{132}\text{I}$ , $^{93}\text{Y}$
2.00-2.05	$^{132}\text{I}$ , $^{88}\text{Kr}$ , $^{135}\text{I}$ , $^{131}\text{M}$ , $^{131}\text{Te}$
2.15-2.20	$^{88}\text{Kr}$ , $^{93}\text{Y}$ , $^{132}\text{I}$
2.35-2.40	$^{88}\text{Kr}$ , $^{142}\text{La}$
2.50-2.55	$^{140}\text{La}$
--100 HOURS COOLING--	
1.90-1.95	$^{132}\text{I}$
2.00-2.05	$^{132}\text{I}$
2.30-2.35	$^{140}\text{La}$
2.50-2.55	$^{140}\text{La}$
--1000 HOURS COOLING--	
2.15-2.20	$^{144}\text{Pr}$
2.30-2.35	$^{140}\text{La}$
2.50-2.55	$^{140}\text{La}$

TABLE VIII  
U-235 THERMAL  
1 HOUR IRRADIATION

GAMMAS		H-2( $\gamma, n$ )H-1 PHOTONEUTRONS	
COEFFICIENT	LAMBDA	COEFFICIENT	LAMBDA
1.8325E+00	1.1330E+00	1.6144E+00	1.1870E+00
5.3910E-01	3.3390E-01	6.9335E-01	3.6661E-01
2.7399E-02	1.4894E-01	3.1369E-02	1.6074E-01
-2.4085E-04	1.8317E-02	-2.8926E-04	1.6074E-02
4.0298E-04	2.2667E-03	4.2422E-04	2.2656E-03
2.0141E-08	1.6886E-04	2.1103E-08	1.8648E-04
NORM. 3.7108E-04		NORM. 3.6372E-07	
RANGE 1-5000 HRS		RANGE 1-5000 HRS	

TABLE VIII (cont)

U-235 THERMAL  
1 DAY IRRADIATION

GAMMAS		H-2( $\gamma$ ,N)H-1 PHOTONEUTRONS	
COEFFICIENT	LAMBDA	COEFFICIENT	LAMBDA
1.3368E+00	1.1838E+00	1.1739E+00	1.2272E+00
7.4391E-01	3.1829E-01	8.5605E-01	3.5017E-01
5.4904E-02	1.3280E-01	5.9394E-02	1.4508E-01
-2.2903E-03	2.0829E-02	-2.5746E-03	1.7816E-02
3.8321E-03	2.2656E-03	3.9344E-03	2.2622E-03
1.8411E-07	1.5609E-04	1.4722E-07	1.2551E-04
NORM. 9.1112E-04		NORM. 9.1384E-07	
RANGE 1-5000 HRS		RANGE 1-5000 HRS	

U-235 THERMAL  
1 MONTH IRRADIATION

GAMMAS		H-2( $\gamma$ ,N)H-1 PHOTONEUTRONS		BE-9( $\gamma$ ,N)BE-8 PHOTONEUTRONS	
COEFFICIENT	LAMBDA	COEFFICIENT	LAMBDA	COEFFICIENT	LAMBDA
1.0459E+00	7.5643E-01	8.8555E-01	8.0732E-01	1.0774E+00	4.1747E-01
5.9618E-01	2.7066E-01	7.5045E-01	3.1041E-01	2.7723E-01	1.0139E-01
5.4153E-02	2.2499E-03	5.4929E-02	2.2406E-03	2.0071E-02	1.1831E-02
2.4772E-06	1.3563E-05	2.1100E-06	1.0000E-35	2.0050E-02	2.2501E-03
NORM. 9.5956E-04		NORM. 9.6208E-07		NORM. 1.3500E-06	
RANGE 1-5000 HRS		RANGE 1-5000 HRS		RANGE 1-1000 HRS	

U-235 THERMAL  
1 YEAR IRRADIATION

GAMMAS		H-2( $\gamma$ ,N)H-1 PHOTONEUTRONS	
COEFFICIENT	LAMBDA	COEFFICIENT	LAMBDA
1.0332E+00	7.5413E-01	8.8618E-01	7.8269E-01
5.8595E-01	2.6961E-01	7.1672E-01	3.0690E-01
6.6623E-02	2.2500E-03	6.7681E-02	2.2370E-03
2.8301E-05	6.3509E-05	2.3498E-05	3.9548E-05
NORM. 9.7238E-04		NORM. 9.7534E-07	
RANGE 1-5000 HRS		RANGE 1-5000 HRS	

U-238 FAST  
1 MONTH IRRADIATION

GAMMAS		H-2( $\gamma$ ,N)H-1 PHOTONEUTRONS		BE-9( $\gamma$ ,N)BE-8 PHOTONEUTRONS	
COEFFICIENT	LAMBDA	COEFFICIENT	LAMBDA	COEFFICIENT	LAMBDA
1.1809E+00	7.4351E-01	1.0125E+00	7.6045E-01	1.0486E+00	4.4836E-01
4.8675E-01	2.5950E-01	6.2617E-01	3.0093E-01	3.1241E-01	9.9905E-02
6.3182E-02	2.2503E-03	6.3404E-02	2.2109E-03	2.5974E-02	1.0670E-02
				2.1955E-02	2.2230E-03
NORM. 7.7368E-04		NORM. 7.7500E-07		NORM. 1.1423E-06	
RANGE 1-1000 HRS		RANGE 1-1000 HRS		RANGE 1-1000 HRS	

TABLE VIII (cont)

PU-239 THERMAL  
1 MONTH IRRADIATION

GAMMAS		H-2( $\gamma$ ,N)H-1 PHOTONEUTRONS		BE-9( $\gamma$ ,N)BE-8 PHOTONEUTRONS	
COEFFICIENT	LAMBDA	COEFFICIENT	LAMBDA	COEFFICIENT	LAMBDA
1.2703E+00	6.7798E-01	1.0691E+00	6.8569E-01	1.0461E+00	4.6686E-01
3.6433E-01	2.4554E-01	5.3031E-01	2.9970E-01	3.1709E-01	9.6683E-02
7.0305E-02	2.2623E-03	6.8607E-02	2.2197E-03	3.2466E-02	1.0837E-02
				2.4173E-02	2.2229E-03
NORM. 6.6216E-04		NORM. 6.8034E-07		NORM. 9.8220E-07	
RANGE 1-1000 HRS		RANGE 1-1000 HRS		RANGE 1-1000 HRS	

PU-239 FAST  
1 MONTH IRRADIATION

GAMMAS		H-2( $\gamma$ ,N)H-1 PHOTONEUTRONS		BE-9( $\gamma$ ,N)BE-8 PHOTONEUTRONS	
COEFFICIENT	LAMBDA	COEFFICIENT	LAMBDA	COEFFICIENT	LAMBDA
1.3695E+00	6.3683E-01	1.1876E+00	6.5410E-01	1.0869E+00	4.7292E-01
2.7707E-01	2.3406E-01	4.4292E-01	2.9748E-01	2.9930E-01	9.5414E-02
5.6462E-02	2.2688E-03	5.3738E-02	2.2276E-03	2.9796E-02	1.0679E-02
				2.1142E-02	2.2175E-03
NORM. 7.9130E-04		NORM. 8.3390E-07		NORM. 1.6098E-06	
RANGE 1-1000 HRS		RANGE 1-1000 HRS		RANGE 1-1000 HRS	

U-233 THERMAL  
1 MONTH IRRADIATION

GAMMAS		H-2( $\gamma$ ,N)H-1 PHOTONEUTRONS		BE-9( $\gamma$ ,N)BE-8 PHOTONEUTRONS	
COEFFICIENT	LAMBDA	COEFFICIENT	LAMBDA	COEFFICIENT	LAMBDA
8.8784E-01	7.1633E-01	8.4783E-01	7.3931E-01	1.1015E+00	3.7857E-01
6.7859E-01	2.6879E-01	7.3718E-01	2.9595E-01	2.3020E-01	1.0349E-01
4.7709E-02	2.2412E-03	4.6976E-02	2.2073E-03	1.9556E-02	1.1687E-02
				1.8774E-02	2.2630E-03
NORM. 1.1051E-03		NORM. 1.1331E-06		NORM. 1.4785E-06	
RANGE 1-1000 HRS		RANGE 1-1000 HRS		RANGE 1-1000 HRS	

TH-232 FAST  
1 MONTH IRRADIATION

GAMMAS		H-2( $\gamma$ ,N)H-1 PHOTONEUTRONS		BE-9( $\gamma$ ,N)BE-8 PHOTONEUTRONS	
COEFFICIENT	LAMBDA	COEFFICIENT	LAMBDA	COEFFICIENT	LAMBDA
9.4558E-01	8.6845E-01	9.3809E-01	8.5712E-01	1.0604E+00	4.1864E-01
7.3537E-01	2.7531E-01	7.4688E-01	2.9488E-01	3.0694E-01	1.3114E-01
4.4938E-02	2.2062E-03	4.5853E-02	2.1873E-03	1.4367E-02	1.8079E-02
				1.9046E-02	2.2600E-03
NORM. 1.3687E-03		NORM. 1.3695E-06		NORM. 1.7594E-06	
RANGE 1-1000 HRS		RANGE 1-1000 HRS		RANGE 1-1000 HRS	

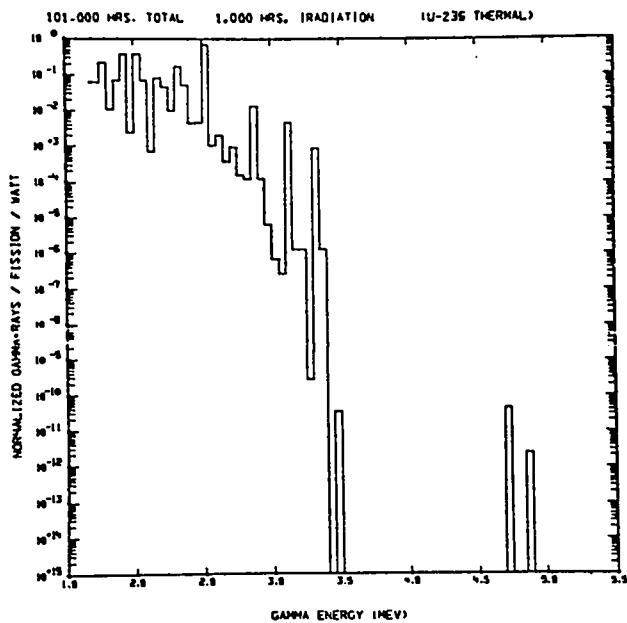


Fig. 7. Gamma spectrum at 1 h irradiation and 100 h cooling (U-235 thermal).

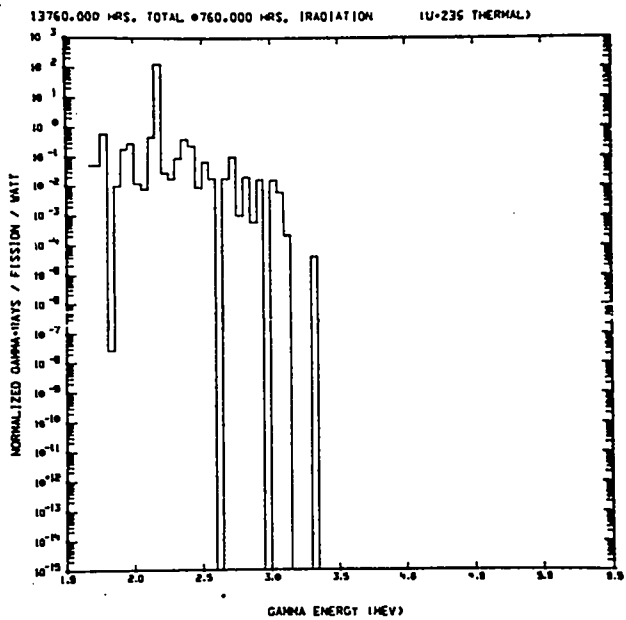


Fig. 9. Gamma spectrum at 1 yr irradiation and 5000 h cooling (U-235 thermal).

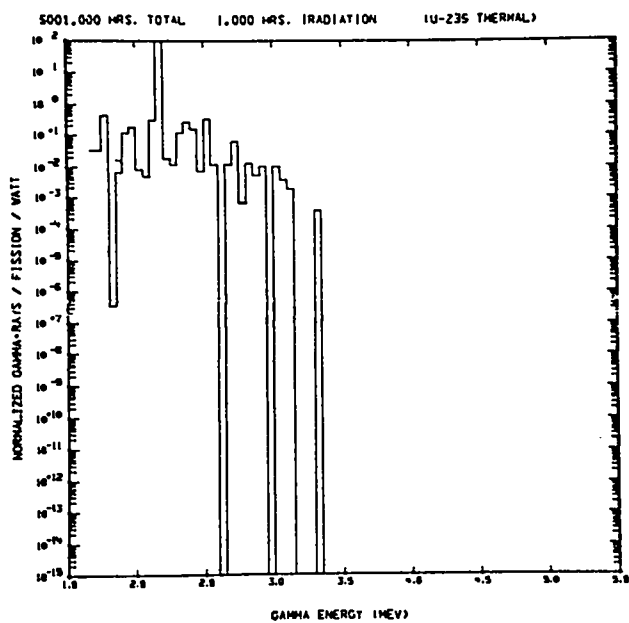


Fig. 8. Gamma spectrum at 1 h irradiation and 5000 h cooling (U-235 thermal).

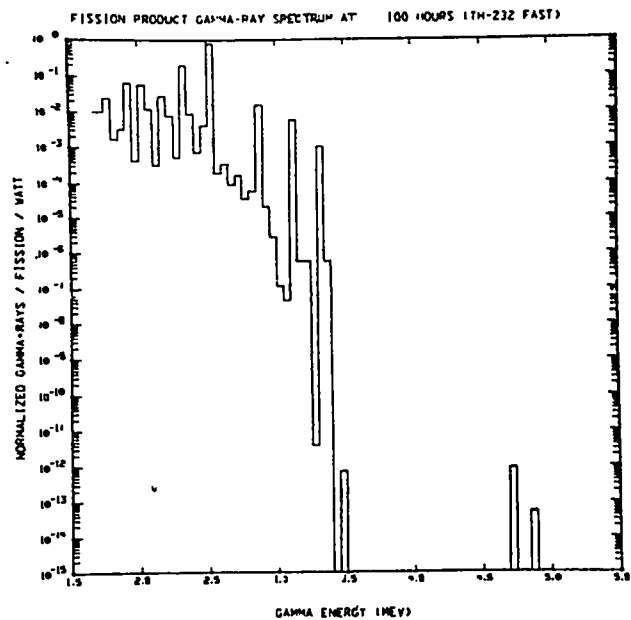


Fig. 10. Gamma spectrum at 1 month irradiation and 100 h cooling (U-235 thermal).

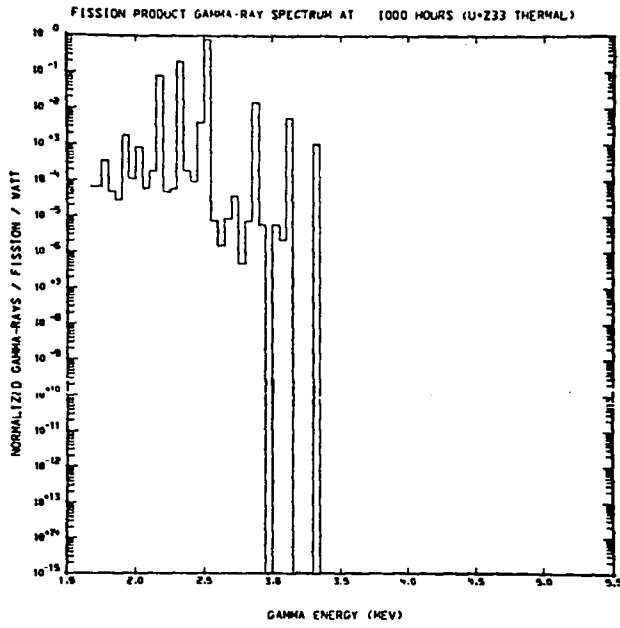


Fig. 11. Gamma spectrum at 1 month irradiation and 1000 h cooling (U-233 thermal).

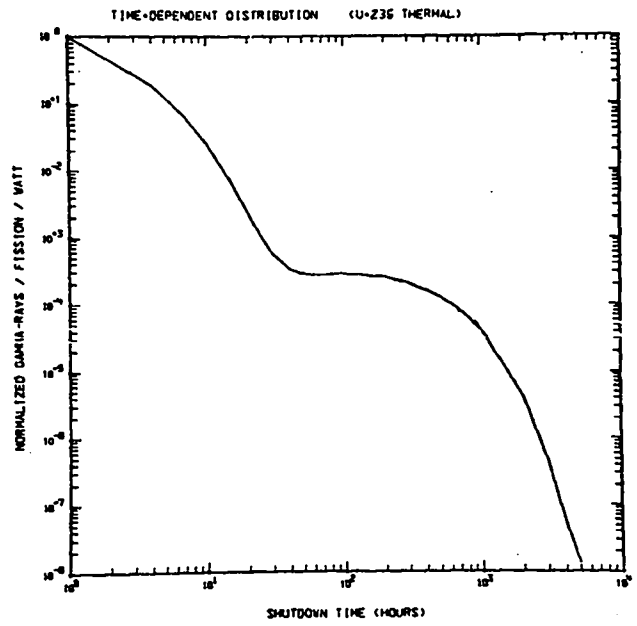


Fig. 13. Gamma source at 1 h irradiation (U-235 thermal).

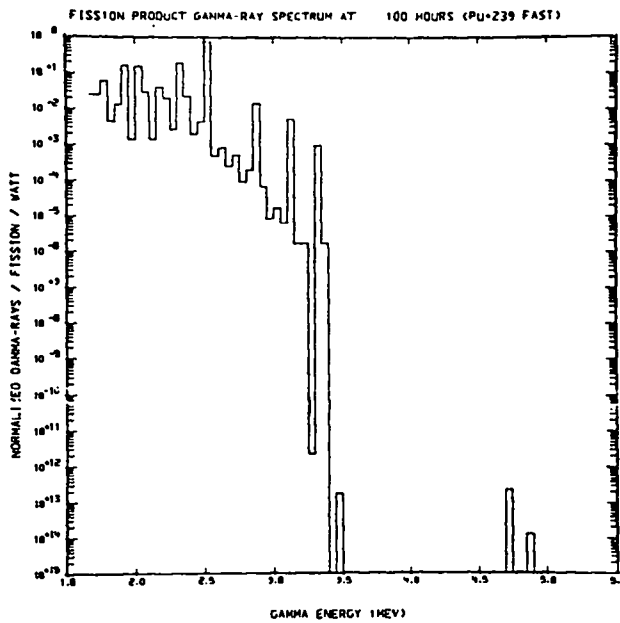


Fig. 12. Gamma spectrum at 1 month irradiation and 100 h cooling (Pu-239 fast).

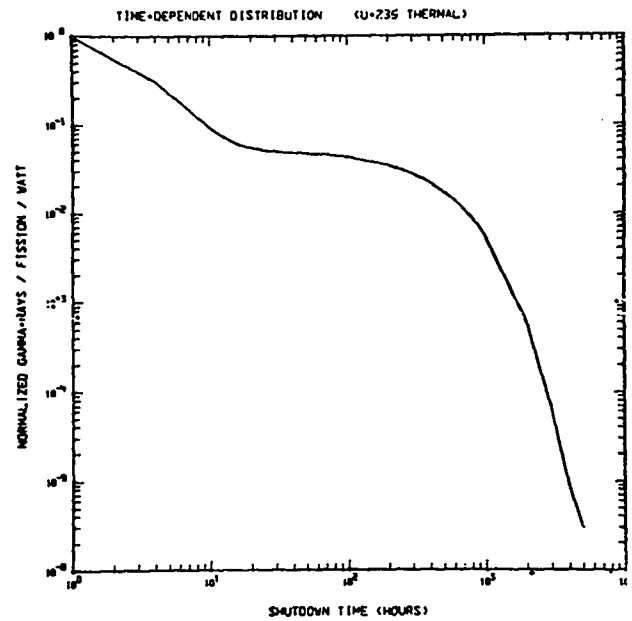


Fig. 14. Gamma source at 1 month irradiation (U-235 thermal).

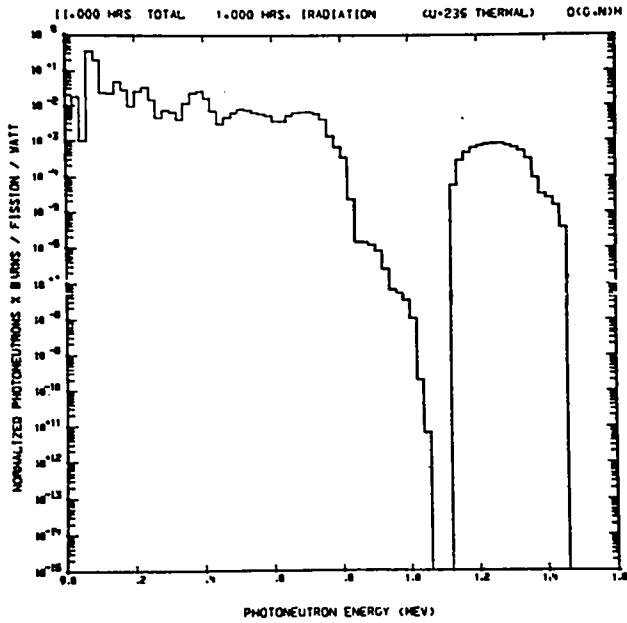


Fig. 15. Photoneutron spectrum at 1 h irradiation and 10 h cooling from  ${}^2\text{H}(\gamma, n){}^1\text{H}$  (U-235 thermal).

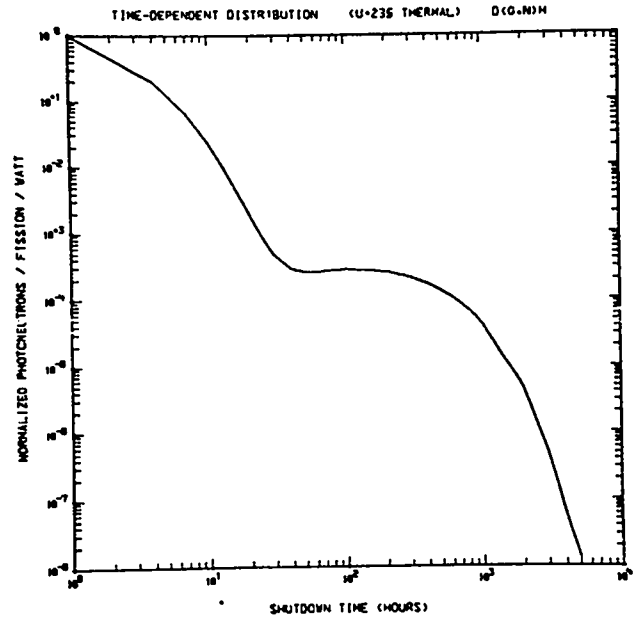


Fig. 17.  ${}^2\text{H}(\gamma, n){}^1\text{H}$  photoneutron source from gamma at 1 h irradiation (U-235 thermal).

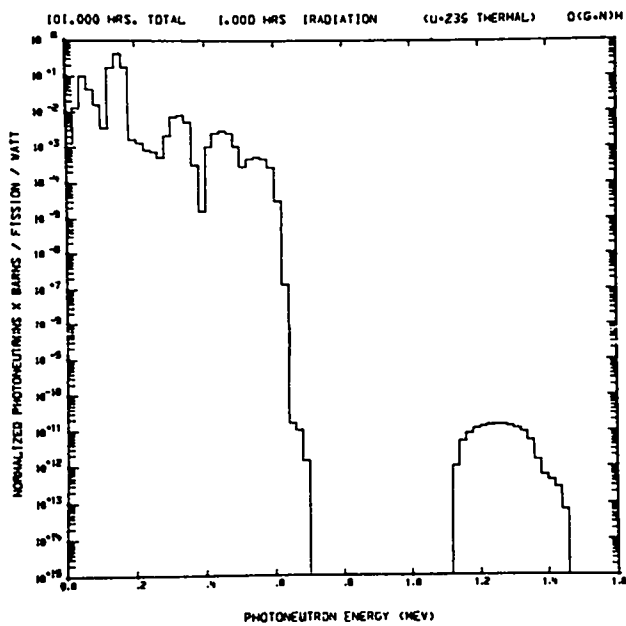


Fig. 16. Photoneutron spectrum at 1 h irradiation and 100 h cooling from  ${}^2\text{H}(\gamma, n){}^1\text{H}$  (U-235 thermal).

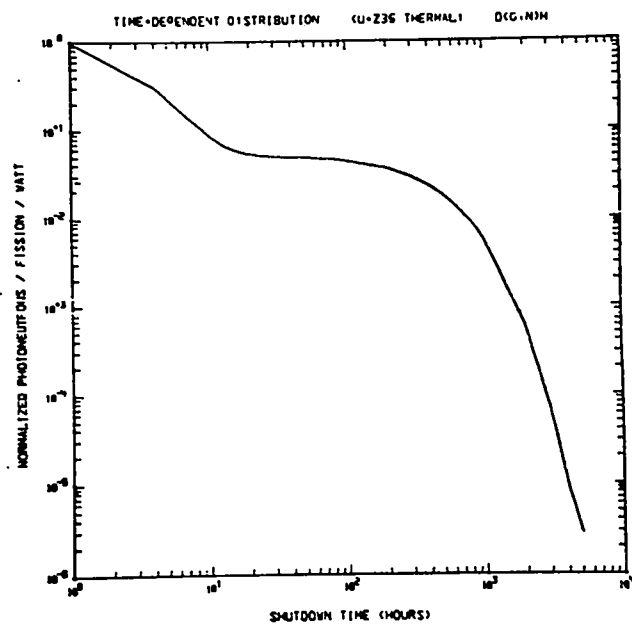


Fig. 18.  ${}^2\text{H}(\gamma, n){}^1\text{H}$  photoneutron source from gamma at 1 month irradiation (U-235 thermal).

VIII. MEDIUM-ENERGY LIBRARY (D. G. Foster, Jr.)

The processor for converting Monte Carlo histories to the National Aeronautics and Space Administration (NASA) working format of equiprobability boundaries is finished, except for a library-management system for storing the output of the processor. As noted last quarter, the pathological nature of the secondary nucleon angular distributions forced us to abandon a Legendre-series representation and resort to direct binning of the histories.

In the revised processor, the output equiprobability-boundary arrays from a previous run are read in to provide an approximate grid for binning. The previous run should be for a similar nucleus at a nearby bombarding energy. The high-energy arrays are scaled in proportion to the bombarding energy to take advantage of the fact that the secondary distributions are almost universal functions of  $E/E_{\text{bomb}}$ . Each scale is then subdivided so as to bracket the equiprobability boundaries as closely as possible, and then the history file is read and the events tallied. Linear interpolation is used to locate the revised boundaries within each bin.

In order to balance running time against the inaccuracy of linear interpolation, the processor can begin by scanning only part of the data and deducing a new starting grid from the partial scan. Up to three iterations are permitted. The entire data set can be scanned a second time to assess the accuracy of the result, at a cost of about 50% more running time.

Since secondary particles from the cascade phase are binned into 400 equally probable bins, the processor is subject to major statistical fluctuation, particularly for secondary mesons near their production thresholds. Accordingly, the processor reads the total number of particles of each type from a card punched by CROIX (the code which generated the histories), scales the numbers for partial scans of the data set, and estimates the number of particles/bin which will result. The degree of subdivision of the preliminary grid is set to maintain a specified minimum for this ratio (currently set at 4/bin). If the expected density with no subdivision at all falls below 4/bin, the input grid is actually thinned before scanning, and the counts/bin subsequently apportioned linearly to generate the full 400 bins. This procedure smooths the distribu-

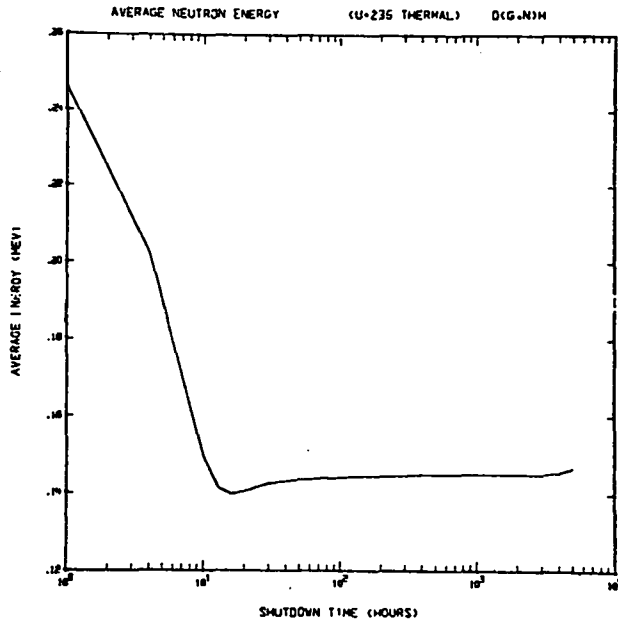


Fig. 19. Average  ${}^2\text{H}(\gamma, n){}^1\text{H}$  photoneutron energy from gammas at 1 month irradiation (U-235 thermal).

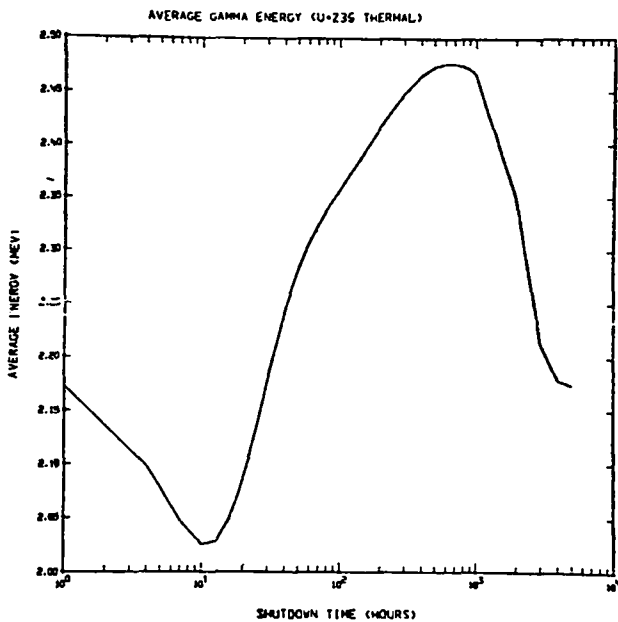


Fig. 20. Average gamma energy at 1 month irradiation (U-235 thermal).

tions so as to give a better representation of the physics. If the memory limits of the computer prevent subdivision to fewer than 8 counts/bin in the narrowest proposed bin, a nonlinear subdivision is used in which the narrowest bins lie next to the preliminary boundaries, and double in width with each step away from the estimated boundaries.

A full-scale test has been run by analyzing 700-MeV protons on  $^{16}\text{O}$  using the output from a full run on 800-MeV protons. Statistically acceptable equiprobability arrays were achieved in a single pass. However, substantially better uniformity was achieved by expending about 25% more running time on one or two preliminary scans of part of the data. The improvement was most marked in the cosine boundaries, for which the statistics are good enough to justify nonlinear subdivision.

#### REFERENCES

1. E. P. Wigner and L. Eisenbud, "Higher Angular Momenta and Long Range Interaction in Resonance Reactions," *Phys. Rev.* 72, 29 (1947); A. M. Lane and R. G. Thomas, "R-Matrix Theory of Nuclear Reactions," *Rev. Mod. Phys.* 30, 257 (1958).
2. G. M. Hale, R. A. Nisley, and D. C. Dodder, Los Alamos Scientific Laboratory, private communication (1975).
3. S. L. Greene, Jr., "Maxwell Averaged Cross Sections for Some Thermonuclear Reactions on Light Isotopes," University of California Radiation Laboratory report UCRL-70522 (1967).
4. D. R. Harris, D. E. Dei, and G. M. Hale, Los Alamos Scientific Laboratory, private communication (1975).
5. C. M. Perey and F. G. Perey, "Compilation of Phenomenological Optical-Model Parameters, 1969-1972," *Atomic Data and Nuclear Data Tables* 13, 293 (1974).
6. B. Zeitnitz, H. Dubenkropp, R. Putzki, G. J. Kirouac, S. Cierjacks, I. Nebe, and Carl B. Dover, "Neutron Scattering from  $^{15}\text{N}$ : (I). R-matrix and Phase-shift Analyses," *Nucl. Phys.* A166, 443 (1971).
7. C. P. Sikkema, "Energy Levels in  $^{16}\text{N}$  from  $^{15}\text{N}(n,n)^{15}\text{N}$  Elastic Scattering," *Nucl. Phys.* 32, 470 (1962).
8. C. K. Cline and M. Blann, "The Preequilibrium Statistical Model: Description of the Nuclear Equilibration Process and Parameterization of the Model," *Nucl. Phys.* A172, 225 (1971).
9. D. G. Foster, Jr. and P. G. Young, "An Evaluation of the Neutron and Photon Production Cross Sections for Aluminum," Los Alamos Scientific Laboratory report LA-4726 (1972).
10. F. C. Maienschein, R. W. Peelle, W. Zobel, and T. A. Love, "Gamma Rays Associated with Fission," *Proc. 2nd Internl. Conf. Peaceful Uses of Atomic Energy (United Nations, Geneva, 1958)* V. 15, p. 366.
11. J. F. Perkins and R. W. King, "Energy Release for the Decay of Fission Products," *Nucl. Sci. Eng.* 3, 726 (1958).
12. P. C. Fisher and L. B. Engle, "Delayed Gamma Rays from Fast-Neutron Fission of  $^{232}\text{Th}$ ,  $^{233}\text{U}$ ,  $^{235}\text{U}$ ,  $^{238}\text{U}$ , and  $^{239}\text{Pu}$ ," *Phys. Rev.* 134, B796 (1964).
13. Odelli Ozer, Ed., "Description of the ENDF/B Processing Codes and Retrieval Subroutines," Brookhaven National Laboratory report BNL-50300 (ENDF 11) (1971).
14. R. E. Schenter, J. L. Baker, and R. B. Kidman, "ETOX, A Code to Calculate Group Constants for Nuclear Reactor Calculations," Battelle Northwest Laboratory report BNWL-1002 (1969).
15. H. Henryson, Argonne National Laboratory, private communication.
16. K. D. Lathrop, "DTF-IV, A FORTRAN-IV Program for Solving the Multigroup Transport Equations with Anisotropic Scattering," Los Alamos Scientific Laboratory report LA-3373 (1965).
17. E. A. Straker, "Suggested Energy Group Bounds for a General Purpose Photon Multigroup Cross Section Set," Science Applications, Inc. report SAI-74-566-HU (1974).
18. C. R. Weisbin, E. M. Oblow, J. Ching, J. E. White, R. Q. Wright, and J. Dreschler, "Cross Section and Method Uncertainties: The Application of Sensitivity Analysis to Study Their Relationships in Computational Benchmark Problems," Oak Ridge National Laboratory report ORNL-TM-4847 (1975).
19. P. G. Young, G. M. Hale, and D. R. Harris, Eds., "Annual Progress Report of the Defense Nuclear Agency Sponsored Cross-Section Evaluation Group," Los Alamos Scientific Laboratory report LA-5759 (1974).
20. C. R. Weisbin and R. J. LaBauve, "Specifications of a Generally Useful Multigroup Structure for Neutron Transport," Los Alamos Scientific Laboratory report LA-5277-MS (1973).
21. R. W. Hardie and W. W. Litte, Jr., 1DX, A One-Dimensional Diffusion Code for Generating Effective Nuclear Cross Sections," Battelle Northwest Laboratory report BNWL-954 (1959).
22. R. E. MacFarlane and Martin Becker, "Self-Shielding of Elastic Transfer Matrices," *Trans. Am. Nucl. Soc.* 21, 495 (1975).
23. B. K. Malaviya, N. N. Kaushal, M. Becker, E. T. Burns, A. Ginsberg, and E. R. Gaerttner, "Experimental and Analytical Studies of Fast Neutron Transport in Iron," *Nucl. Sci. Eng.* 47, 329-348 (1972).

24. R. W. Hardie, R. E. Schenter, and R. E. Wilson, "Evaluation of ENDF/B-IV," Trans. Am. Nucl. Soc. 21, 464 (1975).
25. R. B. Kidman and R. E. Schenter, "Group Constants for Fast Reactor Calculations," Hanford Engineering Development Laboratory report HEDL-TME71-36 (1971).
26. E. D. Cashwell, J. R. Neergard, W. M. Taylor, and G. D. Turner, "MCN: A Neutron Monte Carlo Code," Los Alamos Scientific Laboratory report LA-4751 (1972).
27. R. E. MacFarlane and Martin Becker, "Self-Shielded Cross Sections for Neutron Transport in Iron," to be presented at ANS Winter Meeting, San Francisco (Nov. 1975).
28. D. R. Harris, R. J. LaBauve, R. E. MacFarlane, P. D. Soran, C. R. Weisbin, and J. E. White, "MINX, A Modular Code System for Processing Multigroup Cross Sections from Nuclear Data in ENDF/B Format," Proc. of Seminar on Codes for Nuclear Data Processing, NEA-CPL Ispra (1973).
29. G. I. Bell, G. E. Hansen, and H. A. Sandmeier, "Multitable Treatments of Anisotropic Scattering in Sn Multigroup Transport Calculations," Nucl. Sci. Eng. 28, 376 (1967).
30. B. J. Toppel, D. M. O'Shea, and A. L. Rago, "MC<sup>2</sup> -- A Code to Calculate Multigroup Cross Sections," Argonne National Laboratory report ANL-7318 (1967).
31. W. W. Clendenin, "Calculation of Thermal Diffusion Length and Group Cross Sections: The GLEN Program," Los Alamos Scientific Laboratory report LA-3893 (1968).
32. P. Wälti and P. Koch, "MICROX, A Two-Region Flux Spectrum Code for the Efficient Calculation of Group Cross Sections," Gulf General Atomic report GA-A10827 (1972).
33. P. Wälti, "Evaluation of Grain Shielding Factors for HTGR Coated Fuel Particles," Gulf General Atomic report GAMD-10134 (1970).
34. D. R. Harris, P. G. Young, and G. M. Hale, "Characterization of Uncertainties in Evaluated Cross Sections Sets," Trans. Am. Nucl. Soc. 16, 323 (1973).
35. G. M. Hale, D. R. Harris, and R. E. MacFarlane, Eds., "Applied Nuclear Data Research and Development Quarterly Progress Report," Los Alamos Scientific Laboratory report LA-5944-PR (1975), pp. 11-13.
36. D. R. Harris, W. A. Reupke, and W. B. Wilson, "Consistency Among Differential Nuclear Data and Integral Observations -- The ALVIN Code for Data Adjustment, for Sensitivity Calculations, and for Identification of Inconsistent Data," Los Alamos Scientific Laboratory report (to be published).
37. J. B. Dragt, "Statistical Considerations on Techniques for Adjustment of Differential Cross Sections with Measured Integral Parameters," in "STEK -- the Fast Thermal Coupled Facility at RCN at Petten," Reactor Center of the Netherlands report RCN-122 (1970).
38. H. Häggblom, "Adjustment of Neutron Cross-Section Data by a Least-Square Fit of Calculated Quantities to Experimental Results. Part I. Theory," Aktiebolaget Atomenergi report AE-422 (1971).
39. T. R. England, R. Wilczynski, and N. L. Whittemore, "CINDER-7: An Interim Report for Users," Los Alamos Scientific Laboratory report LA-5885-MS (1975).
40. R. E. Schenter and T. R. England, "Nuclear Data for Calculation of Radioactivity Effects," Trans. Am. Nucl. Soc. 21, 517 (1975).
41. D. R. Marr, "A User's Manual for Computer Code RIBD-II, A Fission Product Inventory Code," Hanford Engineering Development Laboratory report HEDL-TME-75-26 (1975).
42. T. R. England, R. E. Schenter, and N. L. Whittemore, "Delayed Gamma and Beta Energy Release Rates Following <sup>235</sup>U and <sup>239</sup>Pu Fission Bursts," Los Alamos Scientific Laboratory report LA-6021-MS (1975).
43. M. E. Battat, D. J. Dudziak, and H. R. Hicks, "Fission Product Energy Release and Inventory from <sup>239</sup>Pu Fast Fission," Los Alamos Scientific Laboratory report LA-3954 (1968).
44. M. G. Stamatelatos, "PHONEX, A Computer Program to Calculate Photoneutron Spectra," Los Alamos Scientific Laboratory report LA-5860-MS (1975).
45. D. R. Harris, "Natural Reactor Sources," in Naval Reactor Physics Handbook, Vol. I, A. Radkowsky, Ed., 1964, (USAEC TID-7030, 1964), pp. 1085-1142.
46. M. G. Stamatelatos and T. R. England, "Fission-Product Gamma-Ray and Photoneutron Spectra," Conf. on Neutron Cross Sections and Technology, Washington, D. C., March 1975.
47. M. G. Stamatelatos and T. R. England, "Fission-Product  $\gamma$  and  $(\gamma, n)$  Spectra and  $\gamma$  Decay Heat," Trans. Am. Nucl. Soc. 21, 508 (1975).

PUBLICATIONS AND TALKS

1. P. G. Young, "Nuclear Models and Data for Gamma-Ray Production," Invited paper, Conf. on Nucl. Cross Sections and Tech., Washington, D. C., March 1975.
2. G. M. Hale, "R-Matrix Analysis of the Light Element Standards," Invited paper, Conf. on Nucl. Cross Sections and Tech., Washington, D. C., March 1975.

3. N. Jarmie, G. Ohlsen, P. Lovoi, D. Stupin, R. Hardekopf, B. Anderson, J. Sunier, R. Poore, R. Barrett, G. Hale, and D. Dodder, "Elastic Scattering of 7-12 MeV Tritons by Alpha Particles," *Bull. Am. Phys. Soc.* 20, 596 (1975).
4. Leona Stewart, "The  ${}^3\text{He}(n,p)\text{T}$ ,  ${}^6\text{Li}(n,\alpha)\text{T}$  and  ${}^{10}\text{B}(n,\alpha)$  Standard Cross Sections," *Proc. of a Panel on Neutron Standard Ref. Data*, IAEA, Vienna, December 1974.
5. L. Stewart and G. M. Hale, "The  $\text{T}(d,n){}^4\text{He}$  and  $\text{T}(t,n)$  Cross Sections at Low Energies," Los Alamos Scientific Laboratory report LA-5828-MS (USNDC-CTR-2) (1975).
6. S. A. W. Gerstl, D. J. Dudziak, and D. W. Muir, "A Quantitative Assessment of CTR Cross Section Needs," *Conf. on Nucl. Cross Sections and Tech.*, Washington, D. C., March 1975.
7. S. A. W. Gerstl, D. J. Dudziak, and D. W. Muir, "A Quantitative Basis for Cross-Section Requirements for a Fusion Test Reactor," *Trans. Am. Nucl. Soc.* 21, 68 (1975).
8. R. E. Schenter and T. R. England, "Nuclear Data for Calculation of Radioactivity Effects," *Trans. Am. Nucl. Soc.* 21, 517 (1975).
9. T. R. England, R. Wilczynski, and N. L. Whittemore, "CINDER-7: An Interim Report for Users," Los Alamos Scientific Laboratory report LA-5885-MS (1975).
10. M. G. Stamatelatos, "PHONEX, A Computer Program to Calculate Photoneutron Spectra," Los Alamos Scientific Laboratory report LA-5860-MS (1975).
11. M. G. Stamatelatos and T. R. England, "Fission-Product Gamma-Ray and Photoneutron Spectra," *Conf. on Nucl. Cross Sections and Tech.*, Washington, D. C., March 1975.
12. M. G. Stamatelatos and T. R. England, "Fission Product  $\gamma$  and  $(\gamma,n)$  Spectra and  $\gamma$  Decay Heat," *Trans. Am. Nucl. Soc.* 21, 508 (1975).
13. T. R. England, R. E. Schenter, and N. L. Whittemore, "Gamma and Beta Decay Power Following  ${}^{235}\text{U}$  and  ${}^{239}\text{Pu}$  Fission Bursts," Los Alamos Scientific Laboratory report LA-6021-MS (1975).
14. E. M. Bohn, R. J. LaBauve, R. E. Maerker, B. A. Magurno, F. G. McCrossen, and R. E. Schenter, "Benchmark Experiments for Nuclear Data," *Invited paper, Conf. on Nucl. Cross Sections and Tech.*, Washington, D. C., March 1975.
15. D. R. Harris, W. A. Reupke, and W. B. Wilson, "Consistency Among Differential Nuclear Data and Integral Observations--The Alvin Code for Data Adjustment, for Sensitivity Calculations, and for Identification of Inconsistent Data," Los Alamos Scientific Laboratory report LA-5987 (to be published).
16. C. Philis and P. G. Young, "Evaluation des Sections Efficaces des Réactions  ${}^{93}_{41}\text{Nb}(n,2n){}^{92}_{41}\text{Nb}$  et  ${}^{93}_{41}\text{Nb}(n,2n){}^{92}_{41}\text{Nb}$  du Seuil à 20 MeV," *Service de Physique Nucléaire--Centre d'Etudes de Bruyères-le-Châtel report CEA-R-4676* (1975).
17. C. Philis and P. G. Young, "Evaluation de la Section Efficace de la Réaction  ${}^{169}\text{Tm}(n,2n){}^{168}\text{Tm}$  du Seuil à 20 MeV," *Service de Physique Nucléaire--Centre d'Etudes de Bruyères-le-Châtel report*, to be published.
18. R. J. Barrett, "The Regional Energy Assessment Program,"  $\Sigma$  Xi lecture presented at the U. of Idaho (March 1975).
19. E. D. Arthur, W. C. Lam, J. Amato, D. Axen, R. L. Burman, P. Fessenden, R. Macek, J. Oostens, W. Schlaer, S. Sobottka, M. Salomon, and W. Swenson, " $(\pi^+,pp)$  Reaction on Several Light Nuclei," *Phys. Rev.* C11, 332 (1975).
20. Y. Shamai, J. Alster, E. D. Arthur, D. Ashery, S. Cochavi, D. M. Drake, M. A. Moinester, and A. I. Yavin, "The  $(\pi^+, \pi^0)$  Reaction for Light Nuclei in the (3,3) Resonance Region," *Sixth International Conf. on High Energy Physics*, Los Alamos-Santa Fe, 1975.
21. Y. Shamai, J. Alster, E. D. Arthur, D. Ashery, S. Cochavi, D. M. Drake, M. A. Moinester, and A. I. Yavin, "The  ${}^{13}\text{C}(\pi^+, \pi^0)$  Reaction for  $E_n = 30$  to 190 MeV," *Bull. Am. Phys. Soc.* 20, 85 (1975).
22. L. R. Veesser, G. J. Russell, E. D. Arthur, P. A. Seeger, W. F. Sommer, D. M. Drake, and R. G. Fluharty, "Spectrum and Shielding Measurements and Calculations of Neutrons Produced by 800 MeV Protons," *Bull. Am. Phys. Soc.* 20, 155 (1975).
23. E. D. Arthur, D. M. Drake, M. G. Silbert, and P. G. Young, "Fourteen-MeV Neutron-Induced Gamma-Ray Production Cross Sections for Several Elements," *Bull. Am. Phys. Soc.* 20, 166 (1975).
24. D. M. Drake, E. D. Arthur, and D. K. McDaniels, "Radiative Capture Gamma-Rays from the Reaction  ${}^{208}\text{Pb}(n,\gamma){}^{209}\text{Pb}$ ," *Bull. Am. Phys. Soc.* 20, 173 (1975).
25. D. M. Drake, E. D. Arthur, and I. Halpern, "Angular Distributions in the Radiative Capture of 14-MeV Neutrons," *Second International Symposium on Neutron Capture Gamma Ray Spectroscopy*, Petten, The Netherlands, 1974.
26. D. M. Drake, E. D. Arthur, and M. G. Silbert, "More 14-MeV Neutron Induced Gamma-Ray Production Cross Sections," Los Alamos Scientific Laboratory report LA-5893-MS (1975).
27. H. B. Willard, P. R. Bevington, R. J. Barrett, B. D. Anderson, F. Cverna, H. W. Baer, A. N. Anderson, H. Willmes, and N. Jarmie, "Absolute Differential Cross Section Measurements for Proton-Proton Elastic Scattering at 647 and 800 MeV," *Sixth International Conf. on High Energy Physics*, Los Alamos-Santa Fe, 1975.

28. R. J. Barrett, " $\pi^-$  Absorption as a Nuclear Probe," lecture presented at Nuclear Physics Seminar, U. of Idaho, March 1975.
29. A. N. Anderson, R. J. Barrett, and E. A. Wadlinger, "Low Dead-Time Delay-Line Read-Out to Position-Sensitive Proportional Counters," Nucl. Inst. and Meth. 119, 365 (1974).
30. G. M. Hale, D. R. Harris, and R. E. MacFarlane, Eds., "Applied Nuclear Data Research and Development Quarterly Progress Report," Los Alamos Scientific Laboratory reports LA-5804-PR (1974) and LA-5944-PR (1975).
31. C. G. Poncelet, O. Ozer, and D. R. Harris, "Standard, Proprietary, and Government-Supported Nuclear Data Bases," Los Alamos Scientific Laboratory report LA-6023-MS (1975).
32. R. B. Kidman, "FTR Tag Burnup," Trans. Am. Nucl. Soc. 21, 452 (1975).
33. R. B. Kidman, "Europa Heating in Control Rods," Trans. Am. Nucl. Soc. 21, 385 (1975).
34. R. B. Kidman, "Tag Gas Burnup Based on 3-D FTR Analysis," Hanford Engineering Development Laboratory report HEDL-TME-74-58 (1974).
35. R. B. Kidman, "FTR Europa Heating Rates," Hanford Engineering Development Laboratory report HEDL-TME-74-20 (1974).
36. R. E. MacFarlane and Martin Becker, "Self-Shielding of Elastic Transfer Matrices," Trans. Am. Nucl. Soc. 21, 495 (1975).
37. D. W. Muir and D. J. Dudziak, "Sensitivity of RTPR Afterheat and Radioactivity to  $^{94}\text{Nb}$  Cross-Section Uncertainty," Trans. Am. Nucl. Soc. 19, 465 (1974).
38. D. W. Muir, "Sensitivity Analysis for Secondary Energy Distributions," seminar presented at the Radiation Shielding Information Center, Hollifield National Laboratory, February 1975.
39. P. G. Young, "An Evaluation of Gamma-Ray Production Cross Sections from Neutron-Induced Reactions on Tungsten," Los Alamos Scientific Laboratory report LA-5793 (1975).
40. P. G. Young, G. M. Hale, and D. R. Harris, "Annual Progress Report of the Defense Nuclear Agency Sponsored Cross-Section Evaluation Group," Los Alamos Scientific Laboratory report LA-5759-PR (1974).
41. P. G. Young, Ed. "Applied Nuclear Data Research and Development Quarterly Progress Report," Los Alamos Scientific Laboratory report LA-6018-PR (1975).
42. P. G. Young, "Nuclear Data Evaluation at Los Alamos Scientific Laboratory," Seminars presented at Bruyères-le-Châtel, France, June 1974 and EURATOM, Ispra, Italy, July 1974.